NASA CONTRACTOR REPORT

EFFECT OF ABLATION PRODUCT ABSORPTION AND LINE TRANSITIONS ON SHOCK LAYER RADIATIVE TRANSPORT

by K. H. Wilson and H. Hoshizaki

Prepared by
LOCKHEED MISSILES & SPACE COMPANY
Palo Alto, Calif.
for Ames Research Center

NATIONAL AERONAUTICS AND SPACE ADMINISTRATION • WASHINGTON, D. C. • FEBRUARY 1969

EFFECT OF ABLATION PRODUCT ABSORPTION AND LINE TRANSITIONS ON SHOCK LAYER RADIATIVE TRANSPORT

By K. H. Wilson and H. Hoshizaki

Prepared under Contract No. NAS 7-509 by
LOCKHEED MISSILES & SPACE COMPANY
Palo Alto, Calif.

for Ames Research Center

NATIONAL AERONAUTICS AND SPACE ADMINISTRATION

For sale by the Clearinghouse for Federal Scientific and Technical Information
Springfield, Virginia 22151 – CFSTI price $3.00

ACKNOWLEDGMENTS

The authors extend their thanks to Miss H. R. Kirch who performed an indispensable role in developing the computer codes and many of the numerical techniques required in the various solutions. The authors also thank Mr. William Page and Mr. Dale Compton, NASA Ames Research Center for their stimulating discussion, particularly on the problem of radiation transport in atomic lines.

NOMENCLATURE

A	absorption-weighted equivalent width of a line or line group
a_i	velocity profile coefficients
B_ν	Planckian spectral radiant intensity
b_i	velocity profile coefficients, inner layer
C_o	constant in line transport calculation
$C_{\tilde{i}}$	elemental mass fraction of i^{th} element
C_j	mass fraction of j^{th} specie
c	velocity of light
D	diffusion coefficient
D_k	spectral interval covered by an equivalent line
d_k	line spacing with spectral interval D_k
E'	radiative flux divergence
E_{ν_o}	monochromatic continuum emissivity
e	charge on electron, esu
ε_n	exponential integral function
F_1, F_2	functions defined by Eqs. (2.34) and (2.35) respectively
F	radiative flux
f_a	normalized stream function in air layer (inviscid analysis)
f_v	normalized stream function in vapor layer (inviscid analysis)
f_w	blowing parameter
f	normalized tangential velocity function u/u_δ

$\bar{f}$ equivalent line averaged f-number

$f_{nn'}$ line absorption f-number

g normalized total enthalpy function H/H_δ; also function defined by Eq. (4.25)

H total enthalpy

h static enthalpy; also Planck constant

$I_{a,o}; I_{a,1}; I_{a,2}$ mass and momentum flux integrals in air layer (inviscid analysis)

$I_{v,o}; I_{v,1}; I_{v,2}$ mass and momentum flux integral in vapor layer (inviscid analysis

I_o partial mass flux integral (viscous analysis)

I_1 momentum flux integral (viscous analysis)

I radiative intensity

K radius of curvature of reference coordinate surface (inviscid analysis)

$\tilde{K}$ arc-length in x-direction (inviscid analysis)

k_1' rate constant for atomic oxygen-carbon reaction

k_2' rate constant for molecular oxygen-carbon reaction

k_2'' heat of reaction for molecular oxygen-carbon reaction

$\bar{k}$ frozen thermal conductivity

k total thermal conductivity; also Boltzman constant

Le_j Lewis number, Eq. (2.42)

L_1 function defined by Eq. (2.36)

ℓ reciprocal average direction cosine

M_{ij} gms of element i per gram of specie j

$\dot{M}_R$ mass flux due to surface reaction

m mass of electron

$\dot{m}$ mass flux of pyrolysis products

N	number density
n_j	number of lines in equivalent line group
P_1	function defined by Eq. (2.52)
P	pressure
Pr	Prandtl number, Eq. (2.41)
Q_1	function defined by Eq. (2.51)
$Q^{L,C}$	energy emitted by line, absorbed by continuum
$Q^{C,L}$	energy emitted by continuum, absorbed by line
$Q^{L,L}$	energy emitted and absorbed by line
R	body radius
Re_δ	Reynolds number, Eq. (2.16)
r	body radius measured from body centerline
S	integrated line absorption
$Sc_{i,\delta}$	Schmidt number, Eq. (2.29)
T	temperature
U_∞	free-stream velocity
u	velocity component parallel to body
v	velocity component normal to surface
W	equivalent width of a line or group of lines
x	variable in one-dimensional transport calculation
x,y	body-oriented coordinate system
Y_1, Y_2, Y_3	functions defined by Eqs. (2.48), (2.49), (2.50), respectively.
$\bar{\alpha}, \bar{\beta}, \bar{\gamma}$	equivalent line averaged widths
α_o	constant defined by Eq. (2.46) (viscous analysis); also constant defined by Eq. (3.10a) (inviscid analysis)

$\tilde{\alpha}_i$	number of grams of element i per gram of pyrolysis products
β	stagnation point velocity gradient
δ	total physical shock detachment distance (viscous analysis)
$\tilde{\delta}$	total transformed shock detachment distance (viscous analysis)
δ_a	air layer physical thickness (inviscid analysis)
$\tilde{\delta}_a$	air layer transformed thickness (inviscid analysis)
δ_v	vapor layer physical thickness (inviscid analysis)
$\tilde{\delta}_v$	vapor layer transformed thickness (inviscid analysis)
η	transformed normal coordinate
η_v	transformed coordinate at vapor layer edge (viscous analysis)
$\bar{\rho}$	density ratio across shock $\rho'_\infty/\rho'_\delta$
ρ	density
μ	viscosity; also volumetric absorption coefficient
$\tilde{\varkappa}$	arc-length in x-direction (viscous analysis)
$\varkappa$	radius of curvature of reference coordinate surface (viscous analysis)
ϵ	angle between body normal and shock normal
θ	angle between shock normal and symmetry axis; also error integral
Γ_a	function defined by Eq. (3.38)
Γ_v	function defined by Eq. (3.44)
Ω_a	function defined by Eq. (3.39)
Ω_v	function defined by Eq. (3.45)
ξ	normalized x-coordinate
τ_ν	optical depth at frequency ν
ψ	stream function (inviscid analysis)
ω	solid angle; also chemical species source term
ϕ	angle between shock normal and symmetry axis, also error integral

Subscripts

a	air layer properties (inviscid analysis)
$\tilde{a}$	elemental ablation product
$\tilde{i}$	elemental composition
i	i^{th} element
k	equivalent line number
N	nitrogen atom
O	oxygen atom
C	carbon atom
w	body surface quantities
δ	quantities immediately behind shock
∞	free-stream condition
o	line center frequency
v	edge of ablation product layer; also ablation product layer properties (inviscid analysis)

Superscripts

C	continuum contribution
L	line contribution
'	denote dimensional variable, Section 2

Section 1
INTRODUCTION

The radiative gasdynamic problem describing the flow over a blunt body moving at superorbital velocities through the earth's atmosphere has been the subject of a continuing research program (Refs. 1-4). The most recent previous analysis considered the viscous, radiating flow past an ablating body and treated the thermochemical and radiative interaction of the ablation products with the air layer. However, the previous work was limited to relatively low ablation product mass injection rates and, in addition, neglected the radiative energy transported in atomic lines. The present work removes these restrictions by modifying the gasdynamic analysis to handle large mass injection rates and the radiative transport analysis to include lines.

The large mass injection rate problem was approached by two separate analyses. One approach considered a fully viscous flow but treated the velocity field solution in two separate layers. The other approach considered the total shock layer to consist of a distinct inviscid ablation product layer and distinct air layer. An approximate treatment of radiation transport in lines was devised. This approximate treatment uses the concept of "equivalent line" parameters to reduce the numerical calculations to a tractable level. Within the equivalent line approximation a mixture of C, N, and O atomic transitions is included.

Two major conclusions are reached. Firstly, that energy transported in atomic lines is responsible for roughly 50% of the radiative transport within shock layers at conditions typical of superorbital entry. The effect of the increased opacity of high-temperature air due to lines on the surface radiative flux is moderated somewhat by the increased radiation cooling but still results in an increase of 50% in the flux over a continuum-only calculation. Secondly, ablation product species significantly absorb continuum radiative flux from

the high-temperature portion of the shock layer at mass injection levels the order of 5% of the free-stream mass flux. The species primarily responsible for the continuum flux absorption are atomic carbon and hydrogen with molecular species playing a minor role. The ability of ablation product gases to absorb the energy transported in nitrogen and oxygen lines remains to be determined.

Section 2
COUPLED VISCOUS RADIATING FLOW FIELDS

A review of our previously developed analysis (Refs. 2, 3) of the hypersonic flow of a viscous, radiating gas over an ablating blunt body is given. Particular attention is paid to the integral solution of the combined mass and momentum equations for the case of large surface mass injection rates.

2.1 GOVERNING EQUATIONS

In this analysis a direct solution to the radiating, viscous, blunt-body problem is sought. The conservation equations are first simplified by assuming the shock layer to be thin; i.e., $\delta/R \ll 1$. In addition, the thickness of the viscous region is taken to be of the same order of magnitude as the shock-layer thickness. Since the shock detachment distance is $O(\bar{\rho})$ and the thickness of the viscous region is $O(1/\sqrt{Re})$, we have for a viscous shock layer, $\bar{\rho} \sim 1/\sqrt{Re}$. The thin shock-layer equations are also valid when the viscous region is confined to a narrow region near the wall ($\bar{\rho} \gg 1/\sqrt{Re}$).

The approximate equations valid for thin shock layers can be obtained from the conservation equations (cf., Refs. 2, 3) by neglecting all terms of $O(\bar{\rho}^2)$ and higher. The body-oriented coordinate system used in this analysis is shown in Fig. 1. Carrying out the order-of-magnitude analysis results in the following equations valid to $O(\bar{\rho})$.

x-momentum

$$\rho' u' \frac{\partial u'}{\partial x'} + \tilde{\kappa}\rho' v' \frac{\partial u'}{\partial y'} + \kappa'\rho' u' v' = - \frac{\partial P'}{\partial x'} - \frac{1}{\kappa r'} \frac{\partial}{\partial y'} \left[r' u' \tilde{\kappa}^2 \frac{\partial \mu'}{\partial y'} \right] + \frac{\tilde{\kappa}}{r'} \frac{\partial}{\partial y'} \left[\frac{r'}{\tilde{\kappa}} \frac{\partial (\tilde{\kappa}\mu' u')}{\partial y'} \right] \tag{2.1}$$

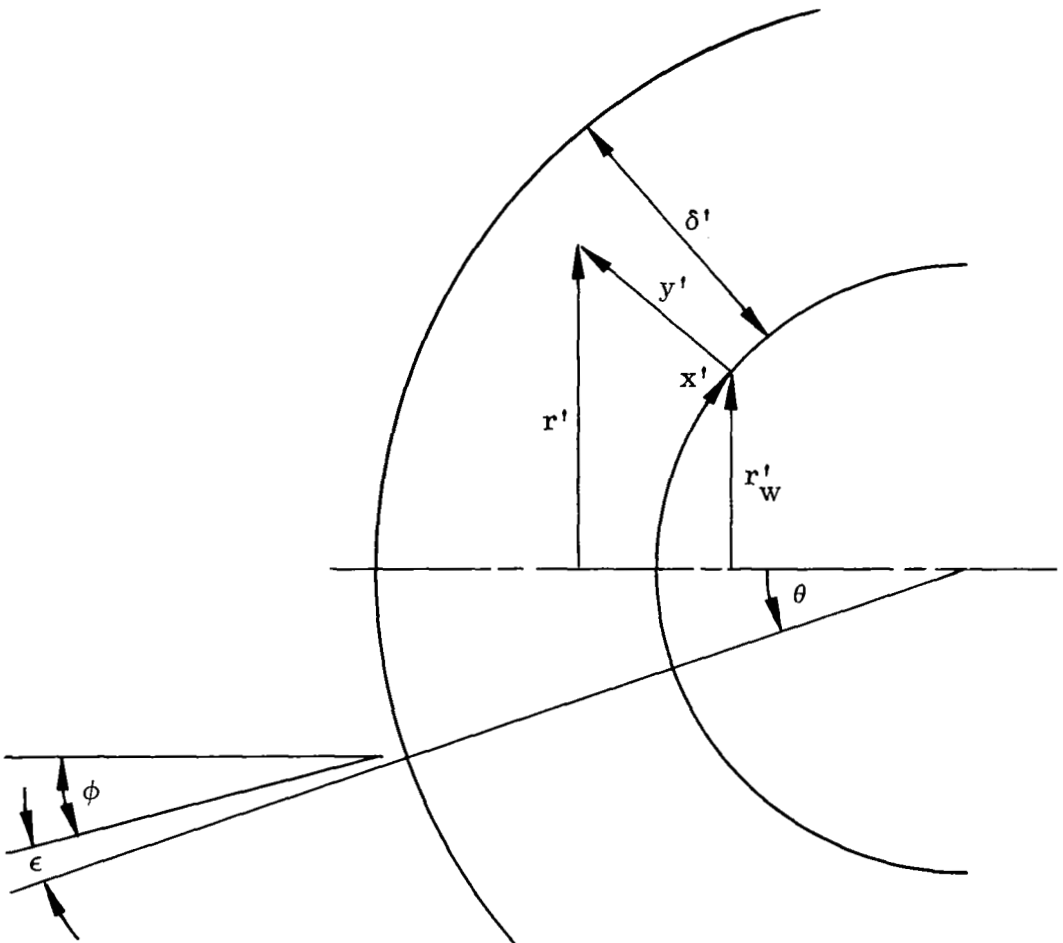

$$\tan \epsilon = \frac{d\delta'}{(1 + \kappa'\delta')\, dx'}$$

$$\delta' = \int_0^{x'} (1 + \kappa'\delta') \tan \epsilon \, dx' + \delta'_o$$

$$r' = r'_w + y' \sin \theta$$

Fig. 1 Body-Oriented Coordinate System

y-momentum

$$\rho'u'\frac{\partial v'}{\partial x'} + \rho'v'\frac{\partial v'}{\partial y'} - \frac{\kappa'\rho'u'^2}{\tilde{\kappa}} = -\frac{\partial P'}{\partial y'} + \frac{4}{3}\frac{\partial}{\partial y'}\left[\frac{\mu'}{r'}\frac{\partial(r'u')}{\partial x'} + \mu'\frac{\partial v'}{\partial y'}\right]$$

$$+ \frac{\partial}{\partial y'}\left(u'\frac{\partial \mu'}{\partial x'}\right) + \frac{\partial u'}{\partial y'}\frac{\partial \mu'}{\partial x'} - \frac{1}{r'}\frac{\partial \mu'}{\partial y'}\frac{\partial(r'u')}{\partial x'} - \frac{1}{r'}\frac{\partial}{\partial x'}\left[r'\frac{\partial(\mu'u')}{\partial y'}\right] \qquad (2.2)$$

Global continuity

$$\frac{\partial}{\partial x'}(r'\rho'u') + \frac{\partial}{\partial y'}(r'\tilde{\kappa}\rho'v') = 0 \qquad (2.3)$$

jth species continuity

$$r'\rho'u'\frac{\partial C_j}{\partial x'} + r'\rho'v'\tilde{\kappa}'\frac{\partial C_j}{\partial y'} = \frac{\partial}{\partial y'}\left[r'\tilde{\kappa}\rho'D'_j\frac{\partial C_j}{\partial y'}\right] + \dot{\omega}_j \qquad (2.4)$$

Energy

$$\frac{\rho'u'}{\tilde{\kappa}}\frac{\partial h'}{\partial x'} + \rho'v'\frac{\partial h'}{\partial y'} = u'\frac{\partial P'}{\partial x'} + v'\frac{\partial P'}{\partial y'} + \frac{1}{\tilde{\kappa}r'}\frac{\partial}{\partial y'}\left[r'\tilde{\kappa}\left\{\bar{k}'\frac{\partial T'}{\partial y'}\right.\right.$$

$$\left.\left. + \Sigma\,\rho'h'_j D'_j \frac{\partial C_j}{\partial y'}\right\}\right] + \mu'\left[\tilde{\kappa}\frac{\partial}{\partial y'}\left(\frac{u'}{\tilde{\kappa}'}\right)\right]^2 - E' \qquad (2.5)$$

For terms of $O(\bar{\rho})$ in the above equations we have set $\tilde{\kappa} = 1$ and $r = r(x)$ to be consistent with our order-of-magnitude approximation. These approximations to the higher order terms are made throughout the analysis. These equations differ slightly from the thin shock-layer equations presented by Hayes and Probstein (Ref. 5) since our analysis is not restricted to stagnation-point flows.

The simplified shock layer equations, Eqs. (2.1)-(2.5) form a set of parabolic partial differential equations. In principal, with initial data given at the

stagnation point, i.e., along the line $x = 0$, these equations can be integrated about the body. Such an approach requires the simultaneous development of the shock boundary by integrating the geometric relation (cf. Fig. 1),

$$d\delta'/dx = (1 + \varkappa'\delta') \tan\varepsilon$$

We have followed an alternative approach in which an initial iterative estimate on the shock curvature $d\phi/dx$ is specified for all x. Note that by twice integrating the shock curvature, the shock-detachment distance is determined to within an arbitrary constant. The arbitrary constant is taken from the stagnation-point solution for $\delta(x = 0)$. The technique of prescribing the shock boundary has more significance than a practical method of solution. Since the governing equations are parabolic with characteristics given by $x = \text{const.}$, then the problem is mathematically not well-set in terms of initial data prescribed along the characteristic, $x = 0$. The specification of boundary data along the "strips" defined by the body and shock leads to a well set problem and one which is stable to numerical integration.

At the stagnation point, symmetry conditions provide all but one boundary condition necessary to determine a solution. The remaining boundary condition is either the stagnation-point shock curvature or shock-detachment distance. In the present analysis the unknown boundary condition is supplied by assuming the shock is concentric to the body at the stagnation point, i.e., $d\phi/dx = d\theta/dx$. The iterative method mentioned above for determining the shock shape for $x > 0$ serves only as a means for obtaining the solution which corresponds to the assumed initial condition at the stagnation point. It does not yield any information about the accuracy of the assumed initial condition. Hence, the solutions are dependent on the assumed initial condition.

The radiation term E' in the energy equation specifies the net emission or absorption of radiant energy per unit volume per unit time. It is calculated assuming the shock layer is locally one-dimensional. That is, for any value of x, temperature and density gradients in the x-direction at all points

across the shock layer are neglected insofar as radiation transport is concerned. In addition, the geometric approximation is made that the shock-layer geometry is that of an infinite plane slab. A derivation of the radiative flux expression under the one-dimensional approximation is given in Section 4. In that discussion methods for including both continuous and discrete (i.e., line) absorption processes are derived. In the development of the energy equation in this section, we will simply treat the quantity E' as a known function of y.

2.2 INTEGRATION OF MOMENTUM EQUATION

In this analysis, solutions to the momentum equation are obtained in an approximate manner by means of an integral method. The velocity profiles resulting from this approximate solution are then used to solve the species continuity and energy equations by means of a modified finite difference method (Ref. 6). The justification for this method of solution rests on the fact that the momentum equation is weakly coupled to the species continuity and energy equation. Approximate velocity and profiles can result in accurate species concentration and total enthalpy profiles if the species continuity and energy equation are solved by finite differences or a similar method.

In carrying out the integral method of solution, the momentum equation is integrated across the shock layer to obtain an integro-differential equation in one independent variable. The integrals are evaluated by assuming that the velocity profile in the shock layer can be represented by suitable polynomials. Before the x-momentum equation is integrated across the shock layer, the viscous terms can be manipulated into a form which is more convenient for integration. Carrying out the manipulation results in

$$\rho' u' \frac{\partial u'}{\partial x'} + \kappa \rho' v' \frac{\partial u'}{\partial y'} + \kappa' \rho' u' v' = - \frac{\partial P'}{\partial x'} + \frac{1}{\tilde{\kappa}} \left(\frac{r'_w}{r'}\right) \frac{\partial}{\partial y'} \left[\tilde{\kappa}^2 \left(\frac{r'}{r'_w}\right) \mu' \frac{\partial u'}{\partial y'} - \kappa' \mu' u' \right] \tag{2.6}$$

The integration of the x-momentum equations follows closely the work of Maslen and Moeckel (Ref. 7), where additional details of the integration technique are presented. The y-momentum equation is used in the integration of the x-momentum to rewrite the pressure gradient term in a form suitable for integration. For this purpose, the y-momentum is reduced to

$$\varkappa' \rho' u'^2 = \frac{\partial P'}{\partial y'} \tag{2.7}$$

since the pressure gradient terms are higher order terms. The terms which have been neglected in Eq. (2.2) are $O(\bar{\rho}^2)$ with respect to the x-momentum equation.

In the analysis to follow, the variables are now nondimensionalized in the following manner:

$$u = \frac{u'}{U'_\infty} \qquad \xi = \frac{x'}{R'} \qquad \delta = \frac{\delta'}{R'} \qquad (\rho v)_w = \frac{(\rho' v')_w}{\rho_\infty U_\infty}$$

$$v = \frac{v'}{U'_\infty} \qquad y = \frac{y'}{R'} \qquad \tilde{\delta} = \frac{\tilde{\delta}'}{R'} \qquad h_\delta = \frac{h'_\delta}{H'_\delta}$$

$$E = \frac{E'R'}{\rho'_\infty (U'_\infty)^3} \qquad \rho = \frac{\rho'}{\rho'_{\delta,o}} \qquad \mu = \frac{\mu'}{\mu'_{\delta,o}} \qquad H'_\delta = \frac{1}{2} U'^2_\infty$$

$$\varkappa = \varkappa' R' \qquad H = \frac{H'}{H'_\delta} \qquad P = \frac{P'}{\rho'_\infty U'^2_\infty}$$

$$\tilde{\varkappa} = 1 + \varkappa y \qquad h = \frac{h'}{h'_\delta} \qquad r = \frac{r'}{R'}$$

The compressibility effects can be reduced significantly by introducing the Dorodnitzyn variable defined by

$$\eta = \frac{\int_o^{y'} (r'/r'_w)\rho' dy'}{\int_o^{\delta} (r'/r'_w)\rho' dy} = \frac{\int_o^{y'} (r'/r'_w)\rho' dy}{\tilde{\delta}} \tag{2.8}$$

Integration of the momentum equation across the shock layer and transformation into the η,ξ variables results in the following integro-differential equations.

momentum

$$\begin{aligned} &\frac{dI_1}{d\xi} + \left[\frac{2}{u_\delta}\frac{du_\delta}{d\xi} + \frac{1}{r_w}\frac{dr_w}{d\xi}(1 + \delta\kappa)\right] I_1 - \left(1 + \frac{\delta\sin\theta}{r_w}\right)\rho_\delta \frac{d\delta}{\delta\xi} \\ &\quad - \frac{d\kappa}{d\xi}\delta^2 \int_o^1 \left(f^2 \int_o^\eta \frac{d\bar{\eta}}{\rho}\right) d\eta + \left[1 + \delta\left(\frac{\sin\theta}{r_w} + 2\kappa\right)\right]\frac{v_\delta \rho_\delta}{u_\delta} \\ &= -\frac{\delta\bar{\rho}}{u_\delta^2}\left(\frac{\partial P}{\partial\xi}\right)_\delta + \frac{1}{\delta u_\delta Re_\delta}\Big[\{1 + 2\delta\left(\frac{\sin\theta}{r_w} + \kappa\right)\}(\rho\mu)_\delta f'(1) - \mu_\delta \delta\kappa \\ &\quad - (\rho\mu)_w f'(0)\Big] \end{aligned} \tag{2.9}$$

where

$$I_1 = \tilde{\delta}\int_o^1 f^2\, d\eta \tag{2.10}$$

$$f = u/u_\delta \tag{2.11}$$

In addition, the following approximation was used to obtain the second term in the momentum equation:

$$\tilde{\kappa}_\delta I_1 \approx \tilde{\delta} \int_0^1 \tilde{\kappa} f^2 \, d\eta$$

A critical point in constructing the integral solution is the selection of the functional form of the tangential velocity profile $f(\eta)$. Clearly the velocity profile can be influenced strongly by surface mass injection. The relative role of the viscous stresses and the convective momentum flux at the wall can be assessed by the injection parameter (Ref. 8),

$$f_w = \frac{\rho'_w v'_w}{\rho'_e u'_e} \sqrt{Re_x} \tag{2.12}$$

Rearranging terms and assuming that the edge conditions in the air layer are essentially those behind the shock, i.e., $\rho_e \sim \rho_\delta$ and $\mu_e \sim \mu_\delta$, then we can express f_w in more convenient terms as

$$f_w = \frac{\dot{m} \, \bar{\rho} \sqrt{Re_\delta}}{\sqrt{2\beta}} \tag{2.13}$$

where

$$\dot{m} = \frac{(\rho'_w v'_w)}{\rho'_\infty U'_\infty} \tag{2.14}$$

$$\bar{\rho} = \frac{\rho'_\infty}{\rho'_\delta} \tag{2.15}$$

$$Re_\delta = \frac{\rho'_\delta U'_\infty R'}{\mu'_\delta} \tag{2.16}$$

and β is the stagnation point tangential velocity gradient parameter*

*For the nearly spherical bodies of interest, $\beta \sim 1/2$.

$$\beta = \frac{1}{2}\frac{d \ln u}{d \ln x}$$

Examination of the solutions to the boundary layer equations with mass injection show that for $f_w \ll 1$ the viscous effects dominate everywhere (Ref. 8). For such problems, a velocity profile characteristic of a zero mass injection solution is appropriate. Previous work (Refs. 2 and 3) has shown that a fifth order polynomial form for $f(\eta)$,

$$f(\eta) = a_0 + a_1\eta + a_2\eta^2 + a_3\eta^3 + a_4\eta^4 + a_5\eta^5 \qquad (2.17)$$

gives accurate values for the primary viscous quantity of interest, viz., the conductive heat flux at the surface. The determination of the six unknown coefficients in Eq. (2.17) as well as the shock layer thickness $\tilde{\delta}$ are determined by satisfying the overall integrated mass and x-momentum equations together with the following five local boundary conditions:

$f = 0$
$f' \Rightarrow$ (x-momentum equation evaluated at wall) @ $\eta = 0$

$f = 1$
$f' \Rightarrow$ (x-momentum equation evaluated at shock) @ $\eta = 1$
$f'' = 0$

The other limiting case is $f_w \gg 1$ under which the inner layer near the surface* is dominated by inviscid terms. In order to provide a reasonable velocity distribution at large injection rates we have elected to divide the shock layer into two layers: an inner ablation layer and an outer air layer. The point defining the boundary of the two layers is taken to be the value of the transformed shock layer coordinate η_v at which the mass fraction of ablation products becomes less than 1%. By this definition all

*Examination of the diffusion equation shows that the inner layer for $f_w \gg 1$ is essentially composed of ablation product gases.

viscous effects are contained essentially in the inner layer. Both second order and third order polynomial velocity distributions were examined. By virtue of the essentially inviscid nature of the outer layer, a linear velocity profile was selected. The velocity profiles then are

$$0 \le \eta \le \eta_v$$

$$f_{inner} = a_o + a_1\eta + a_2\eta^2 + a_3\eta^3 \tag{2.18a}$$

or

$$f_{inner} = a_o + a_1\eta + a_2\eta^2 \tag{2.18b}$$

and

$$\eta_v \le \eta \le 1$$

$$f_{outer} = b_o + b_1\eta \tag{2.19}$$

The coefficients in Eqs. (2.18) and (2.19) are determined by satisfying the overall integrated x-momentum equation together with the local boundary conditions for Eq. (2.18a) or (2.18b)

$$f_{outer} = 1 \qquad @\ \eta = 1$$

$$f_{outer} = \text{(x-momentum equation evaluated at shock)}$$

$$f_{inner} = f_{outer} \qquad @\ \eta = \eta_v$$

$$f_{inner} = 0 \text{ (normal mass injection)} \qquad @\ \eta = 0$$

$$f'_{inner} = \text{(x-momentum equation evaluated at wall)}$$

and for Eq. (2.18a) the following additional boundary condition was added:

$$f'_{inner} = f'_{outer} \qquad @\ \eta = \eta_v$$

A comparison of the velocity profiles obtained for entry conditions of ($U_\infty = 5 \times 10^4$ ft/sec, $\rho_\infty = 3.98 \times 10^{-7}$ slugs/ft^3, R = 9.0 ft) assuming both a cubic (Eq. (2.18a)) or a quadratic (Eq. (2.18b)) polynomial distribution is shown in Fig. 2. The mass injection rate considered was $\dot{m} = 0.10$ for which the blowing parameter has the value $f_w = 5.6$. Also shown on Fig. 2 are the velocity distributions obtained by De Rienzo and Pallone (Ref. 9) using an exact numerical solution to the boundary layer equations for blowing rates of $f_w = 1.9$ and .95. While these blowing rates are substantially lower than the value of $f_w = 5.6$ being considered for our viscous layer solution, nonetheless, these boundary layer calculations are the only exact mass injection solutions available for the velocities and mass injection rates of interest. It can be seen that neither the quadratic or cubic profile is entirely satisfactory but of the two the quadratic is preferred. For this reason, a quadratic profile was used for all remaining calculations discussed in this report. It appears that significant improvement over the quadratic profile would require the difficult approach of an exact numerical solution to the momentum equations.

2.3 SPECIES CONTINUITY EQUATION

The continuity equations (Eq. (2.4)) for the numerous species considered in this analysis are not solved explicitly. Instead we adopt the elemental approach (Ref. 10) in which the species continuity equation for each element is satisfied. Once the elemental concentration is known, the concentration of the molecular, atomic and ionic species are determined by means of an equilibrium thermodynamic calculation (Ref. 4).

In the present analysis, four elements are considered, viz., oxygen, nitrogen, carbon and hydrogen. The continuity equation, in terms of the elemental mass fractions (denoted by $C_{\tilde{C}}$), can be obtained by multiplying the continuity equation for species j (Eq (2.4)) by $M_{i,j}$ (the number of grams of element

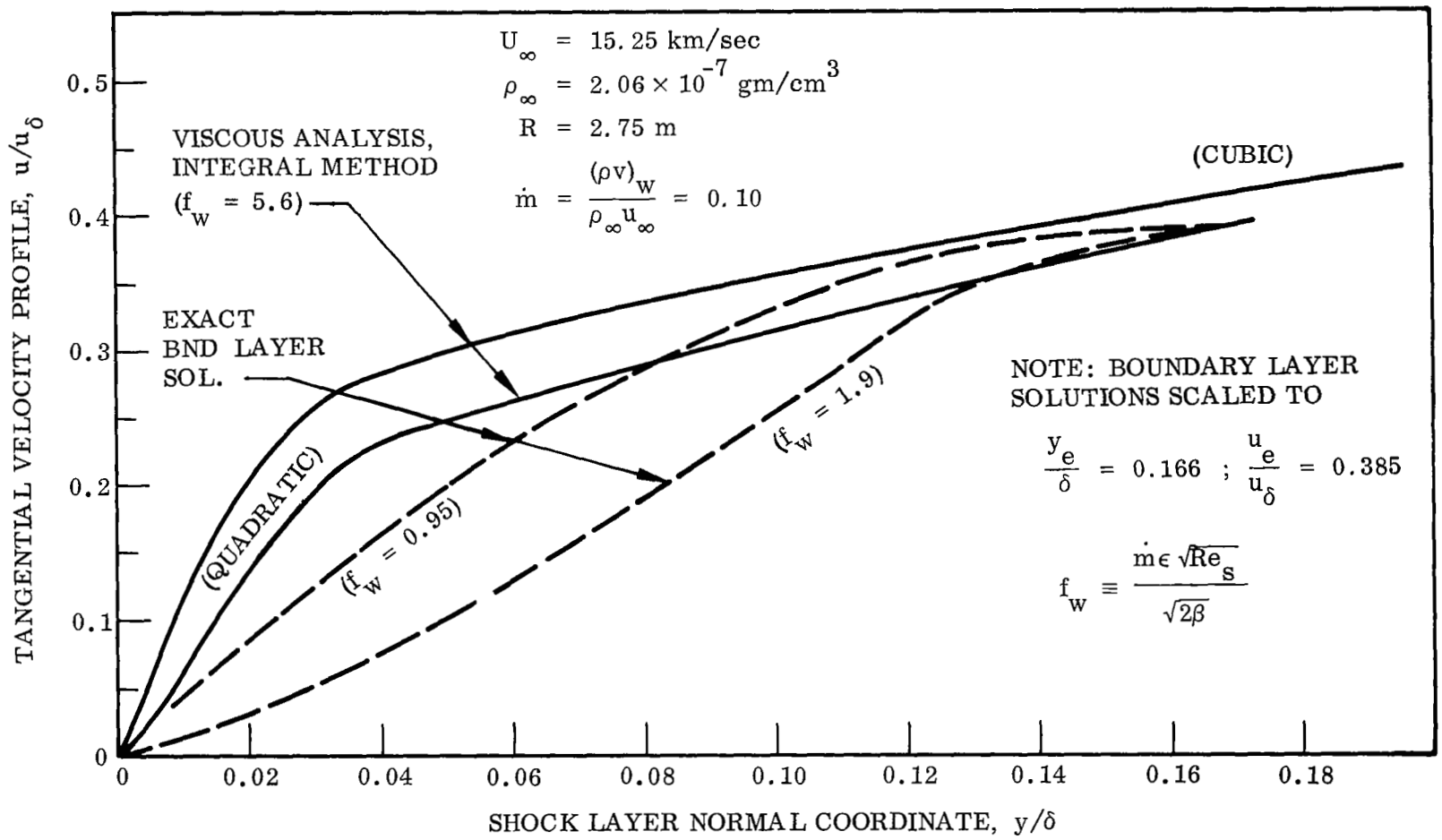

Fig. 2 Comparison of Velocity Profiles from Viscous Analysis (Integral Method) with Exact Boundary Layer Calculations

i per gram of species j) and summing over all species j which contain the element i. Carrying out the summation (see Ref. 4 for details) the elemental species continuity equation can be written as (one for each element i)

$$r'\rho'u' \frac{\partial C_{\tilde{i}}}{\partial x'} + r'\rho'v' \tilde{\pi} \frac{\partial C_{\tilde{i}}}{\partial y'} = \frac{\partial}{\partial y'} \left[r'\tilde{\pi}\, \rho' \sum_j D_j M'_{i,j} \frac{\partial C_j}{\partial y'} \right] \qquad (2.20)$$

since, barring nuclear transformations, $\sum_j M_{i,j}\, \dot{\omega}_j = 0$. Since we have that $\sum_{\tilde{i}} C_{\tilde{i}} = 1$, only three equations of the type Eq. (2.20) are independent. The three elements chosen to be described by Eq. (2.20) were O, N, and C. In order to eliminate the species dependent diffusion term we have assumed that the effective binary diffusion coefficient is the same for each species. Since the diffusion coefficients are inversely proportional to the square root of the reduced molecular weights, this approximation is acceptable as long as the molecular weights of the species are similar. When light elements such as hydrogen are present, this approximation can be quite poor in terms of shock layer species distributions. However the single diffusion coefficient approximation is felt to provide valid results for radiative and convective heat transfer. This point will be discussed further in Section 5.

Using the single diffusion coefficient approximation, Eq. (2.20) becomes

$$r'\rho'u' \frac{\partial C_{\tilde{i}}}{\partial x'} + r'\rho'v' \tilde{\pi}' \frac{\partial C_{\tilde{i}}}{\partial y'} = \frac{\partial}{\partial y'} \left[r'\tilde{\pi}\rho' D'_{\tilde{i}} \frac{\partial C_{\tilde{i}}}{\partial y'} \right] \qquad (2.21)$$

Two boundary conditions are necessary to determine the species concentration variation across the shock layer. The first boundary condition is that the injected species concentration is zero at the shock. The second boundary condition is obtained from a mass balance at the wall. The total mass flux at the surface is

$$\rho'v' = \alpha_{\tilde{O}}\dot{m}' + \alpha_{\tilde{H}}\dot{m}' + \alpha_{\tilde{N}}\dot{m}' + \alpha_{\tilde{C}}\dot{m}' + \dot{M}'_R \qquad (2.22)$$

where $\dot{m}'$ is the mass flux of the pyrolysis product,* $\alpha_{\tilde{O}}$ is the number of grams of oxygen per gram of pyrolysis product (similar definitions for $\alpha_{\tilde{H}}$, $\alpha_{\tilde{N}}$ and $\alpha_{\tilde{C}}$) and $\dot{M}_R'$ is the mass flux associated with surface reactions. We will consider charring ablators where the char is pure carbon. Only two surface reactions will be considered and these reactions will be assumed to produce carbon monoxide. The surface reactions considered are (Ref. 4)

$$C_{(s)} + O_{(g)} \xrightarrow{k_1'} CO_{(g)} \tag{2.23}$$

$$C_{(s)} + 1/2\ O_{2(g)} \xrightarrow{k_2'} CO_{(g)}$$

so that

$$\dot{M}_R' = \rho' M_C' T'^{1/2} \left(k_1' \frac{C_O}{M_O'} + k_2' \frac{C_{O_2}}{M_O'} e^{-k''_2/T'}\right) \tag{2.24}$$

Mass balances at the surface for the elements yield

$$C_{\tilde{O}} (\rho' v') - \rho' D_{\tilde{O}}' \frac{\partial C_{\tilde{O}}}{\partial y'} = \alpha_{\tilde{O}} \dot{m}' \tag{2.25}$$

$$C_{\tilde{N}} (\rho' v') - \rho' D_{\tilde{N}}' \frac{\partial C_{\tilde{N}}}{\partial y'} = \alpha_{\tilde{N}} \dot{m}' \tag{2.26}$$

$$C_{\tilde{C}} (\rho' v') - \rho' D_{\tilde{C}}' \frac{\partial C_{\tilde{C}}}{\partial y'} = \alpha_C \dot{m}' + \dot{M}_R' \tag{2.27}$$

In terms of nondimensional variables and transforming to ξ, η coordinates, the elemental species continuity equation is

*The mass flux of the pyrolysis product is assumed to be a known quantity. In general, it can be obtained from an energy balance at the surface.

$$\frac{\partial}{\partial\eta}\left[(\rho/\rho_\delta)^2\left(\frac{r}{r_w}\right)^2\frac{\tilde{\varkappa}}{S_{c_{i,\delta}}}\frac{\partial C_{\tilde{i}}}{\partial\eta}\right]+\tilde{\delta}\,Re_\delta u_\delta\left[\frac{\partial I_o}{\partial\xi}+I_o\left(\frac{1}{u_\delta}\frac{du_\delta}{d\xi}\right.\right.$$

$$\left.\left.+\frac{1}{r_w}\frac{dr_w}{d\xi}\right)-\dot{m}\frac{\bar{\rho}}{u_\delta}\right]\frac{\partial C_{\tilde{i}}}{\partial\eta}=Re_\delta\,\tilde{\delta}^2 u_\delta\, f\frac{\partial C_{\tilde{i}}}{\partial\xi} \tag{2.28}$$

where

$$S_{c_{i,\delta}}=\frac{\mu'_{\mu,o}}{\rho'_{\delta,o}D'} \tag{2.29}$$

$$Re_\delta=\frac{\rho'_{\delta,o}U'_\infty R'}{\mu'_{\delta,o}} \tag{2.30}$$

The normal flux was obtained by integrating the global continuity equation.

$$\tilde{\delta}f\frac{\partial\eta}{\partial\xi}+\left(\frac{r}{r_w}\right)\varkappa\frac{\rho v}{u_\delta}=-\frac{\partial I_o}{\partial\xi}-I_o\frac{\partial/\partial\xi(u_\delta r_w)}{u_\delta r_w}+\frac{(\rho v)_w}{u_\delta} \tag{2.31}$$

The quantity $I_o(\eta)$ is defined by

$$I_o=\tilde{\delta}\int_o^\eta f\,d\eta \tag{2.32}$$

Eq. (2.28) is of the form

$$\frac{\partial}{\partial\eta}\left[\frac{1}{F_1}\frac{\partial C_{\tilde{i}}}{\partial\eta}\right]+\left[\frac{1}{F_1}\frac{\partial C_{\tilde{i}}}{\partial\eta}\right]F_2=L_1 \tag{2.33}$$

where

$$F_1=\frac{S_{c_{i,\delta}}}{\tilde{\varkappa}\left(\frac{r}{r_w}\right)^2\left(\frac{\rho}{\rho_{\delta,o}}\right)} \tag{2.34}$$

$$F_2 = u_\delta F_1 \tilde{\delta} \, Re_\delta \left[\frac{\partial I_o}{\partial \xi} + I_o \left(\frac{1}{u_\delta} \frac{du_\delta}{d\xi} + \frac{1}{r_w} \frac{dr_w}{d\xi} \right) - \frac{\bar{\dot{m}}}{u_\delta} \right] \tag{2.35}$$

$$L_1 = Re_\delta \, \tilde{\delta} \, u_\delta \, f \left(\frac{\partial C_{\tilde{i}}}{\partial \xi} \right) \tag{2.36}$$

The solution for $C_{\tilde{i}}$ is

$$C_{\tilde{i}} = \int_o^\eta \left[F_1 \int_o^\eta L_1 e^{-\int_{\eta'}^{\eta} F_2 d\eta'} \, d\eta + F_1 C_1 e^{-\int_o^\eta F_2 d\eta} \right] d\eta + C_2 \tag{2.37}$$

where the constants of integration (C_1 and C_2) are determined from the two boundary conditions discussed previously.

2.4 ENERGY EQUATION

It is somewhat more convenient in carrying out the numerical solution to rewrite the energy equation in terms of total enthalpy. Combining the momentum equations (Eqs. (2.6) and (2.7)) with the energy equation written in terms of the static enthalpy (Eq. (2.5)) results in

$$\begin{aligned} \frac{\rho' u'}{\tilde{\varkappa}} \frac{\partial H'}{\partial x'} + \rho' v' \frac{\partial H'}{\partial y'} = {} & \frac{1}{\tilde{\varkappa}} \left(\frac{r_w'}{r'} \right) \frac{\partial}{\partial y'} \left[\tilde{\varkappa}^2 \frac{r'}{r_w'} \mu' \frac{\partial (u'^2/2}{\partial y'} \right] \\ & - \varkappa' \frac{\partial}{\partial y'} (\mu' u'^2) \\ & + \frac{1}{\tilde{\varkappa}} \frac{r_w'}{r'} \frac{\partial}{\partial y'} \left[\frac{r'}{r_w'} \tilde{\varkappa} \left(\bar{k}' \frac{\partial T'}{\partial y} + \rho' \sum_j D_j' h_j' \frac{\partial C_j}{\partial y'} \right) \right] - E' \end{aligned} \tag{2.38}$$

The diffusion term, which represents the transport of enthalpy by diffusion, requires discussion. Although one can argue that the diffusion coefficient for each species is similar, the enthalpy for each species, h_j', varies widely for the species considered. Hence, it becomes necessary to evaluate the enthalpy transported by diffusion by each species j.

The evaluation of the species concentration gradients presents some difficulty. The gradients can be written as

$$\frac{\partial C_j(T',P',C_{\tilde{i}}}{\partial y'} = \frac{\partial C_j}{\partial T'}\frac{\partial T'}{\partial y'} + \sum_{\tilde{i}}^{4}\frac{\partial C_j}{\partial C_{\tilde{i}}}\frac{\partial C_{\tilde{i}}}{\partial y'} \tag{2.39}$$

where we have neglected the effect of pressure on the grounds that the temperature gradients are much larger than pressure gradients. Using Eq. (2.39) then after some manipulation, the energy equation can be written as

$$\rho'\frac{r'}{r'_w}\left(u'\frac{\partial H'}{\partial x'} + \tilde{\nu}\,v'\frac{\partial H'}{\partial y'}\right) = \frac{\partial}{\partial y'}\left[\frac{r'}{r'_w}\tilde{\nu}\left\{\frac{\mu'}{P_r}\frac{\partial h'}{\partial y'} + \mu'\frac{\partial(u'^2/2)}{\partial y'}\right.\right. \tag{2.40}$$

$$\left.\left. + \frac{\mu'}{P_r}\sum_{\tilde{i}=1}^{4}\sum_{j}(Le_j-1)\,h'_j\frac{\partial C_j}{\partial C_{\tilde{i}}}\frac{\partial C_{\tilde{i}}}{\partial y'}\right\}\right] - \nu'\frac{\partial}{\partial y'}(\mu'u'^2) - E'\tilde{\nu}\frac{r'}{r'_w}$$

In obtaining Eq. (2.40) we have used the "total" properties in defining the Prandtl and Lewis numbers, viz., (Ref. 4)

$$P_r = C'_p\,\mu'/k' \tag{2.41}$$

$$Le_j = \frac{\rho' C'_p D'_j}{k'} \tag{2.42}$$

where

$$C'_p = \bar{C}'_p + \sum_j h'_j\frac{\partial C_j}{\partial T'} \tag{2.43}$$

$$k' = \bar{k}' + \rho'\sum_j D'_j\,h'_j\frac{\partial C_j}{\partial T'} \tag{2.44}$$

The calculation of the concentration derivatives $\partial C_j/\partial C_{\tilde{i}}$ is quite difficult (see Ref. 4). However, within the framework of the single diffusion coefficient approximation we find that $Le_j \approx 1$ and a posterori calculations have shown

that the term

$$\frac{\mu'}{P_r} \sum_i \sum_j (Le_j - 1)\, h_j' \frac{\partial C_j}{\partial C_{\tilde{i}}} \frac{\partial C_{\tilde{i}}}{\partial y'}$$

is negligible.

Again as in Section 2.3, we introduce nondimensional variables and transform to η, ξ coordinates. After considerable manipulation Eq. (2.40) becomes

$$\frac{\partial}{\partial \eta}\left[\left(\frac{r}{r_w}\right)^2 \left(\frac{\rho\mu}{\rho_\delta \mu_\delta}\right) \frac{\tilde{\kappa}}{P_r} \frac{\partial g}{\partial \eta}\right] + Re_\delta\, \tilde{\delta}\, u_\delta \left[\frac{\partial I_o}{\partial \xi} + I_o \frac{d \ln u_\delta r_w}{d\xi} - \frac{\dot{m}\,\bar{\rho}}{u_\delta}\right] \frac{\partial g}{\partial \eta}$$

$$= Re_\delta\, \tilde{\delta}\, u_\sim\, f \frac{\partial g}{\partial \xi} + u_\delta^2 \frac{\partial}{\partial \eta}\left[\left(\frac{r}{r_w}\right)^2 \left(\frac{\rho\mu}{\rho_\delta \mu_\delta}\right) \frac{\tilde{\kappa}}{P_r} (1 - P_r)\, 2f \frac{df}{d\eta}\right] \qquad (2.45)$$

$$+ 2\tilde{\delta}\, u_\delta^2 \frac{\partial}{\partial \eta}\left[\left(\frac{\mu}{\mu_\delta}\right) f^2\right] + \frac{Re_\delta\, \tilde{\delta}\, \bar{\rho}}{\alpha_o} \left(\frac{E'}{\rho}\right)$$

where $g \equiv H/H_\delta$ and the constant α_o is

$$\alpha_o \equiv \frac{\rho_\infty' U_\infty'^3}{2R'} \qquad (2.46)$$

Equation (2.45) has the form,

$$\frac{\partial}{\partial \eta}\left[Y_1 \frac{\partial g}{\partial \eta}\right] + \frac{P_1}{Y_1}\left[Y_1 \frac{\partial g}{\partial \eta}\right] + \frac{\partial Y_2}{\partial \eta} + \frac{\partial Y_3}{\partial \eta} = Q_1 \qquad (2.47)$$

where

$$Y_1 = \left[\left(\frac{\rho\mu}{\rho_\delta \mu_\delta}\right)\left(\frac{r}{r_w}\right)^2 \frac{\tilde{\kappa}}{P_r}\right] \qquad (2.48)$$

$$Y_2 = 2Y_1 (1 - P_r) u_\delta^2 f \frac{df}{d\eta} \tag{2.49}$$

$$Y_3 = 2\tilde{\delta} u_\delta^2 \left(\frac{\mu}{\mu_\delta}\right) f^2 \tag{2.50}$$

$$Q_1 = re_\delta \tilde{\delta}^2 \left[u_\delta f \frac{\partial g}{\partial \xi} + \frac{\bar{\rho}}{\alpha_o} \left(\frac{E'}{\rho}\right)\right] \tag{2.51}$$

$$P_1 = Re_\delta \tilde{\delta} u_\delta \left[\frac{\partial I_o}{\partial \xi} + I_o \frac{d \ln}{d\xi} u_\delta r_w - \frac{\dot{m} \bar{\rho}}{u_\delta}\right] \tag{2.52}$$

The boundary conditions on Eq. (2.47) are the known values of g at the wall and immediately behind the shock, viz.,

$$g = g_w \qquad @ \ \eta = 0$$

$$g = 1 \qquad @ \ \eta = 1$$

Then the solution to Eq. (2.47) is

$$g = g_w + \int_o^\eta \frac{\partial g}{\partial \eta} d\eta \tag{2.53}$$

where

$$\frac{\partial g}{\partial \eta} = \frac{1}{Y_1} \left\{ \int_o^\eta \left(Q_1 - \frac{P_1 Y_2}{Y_1} - \frac{P_1 Y_3}{Y_1} e^{-\int_{\eta'}^\eta \frac{P_1}{Y_1} d\eta''} d\eta' \right. \right. \tag{2.54a}$$

$$\left. \left. + Y_2(\eta) + Y_3(\eta) + C_1 e^{-\int_o^\eta \frac{P_1}{Y_1} d\eta'} \right\} \right.$$

and

$$C_1 = \frac{(1-g_w) - \int_o^1 Y_2 \left[\int_o^\eta \left(Q_1 - \frac{P_1 Y_2}{Y_1} - \frac{P_1 Y_3}{Y_1}\right) e^{-\int_{\eta'}^\eta \frac{P_1}{Y_1} d\eta''} d\eta' + Y_2(\eta) + Y_3(\eta) \right] d\eta}{\int_o^1 Y_2 e^{-\int_o^\eta \frac{P_1}{Y_1} d\eta'}} \tag{2.54b}$$

2.4 NUMERICAL METHODS

The numerical methods separate into two parts. One part is the determination of the shock wave shape and the other part is the determination of the shock layer flow field structure. Although the analysis presented in this section is valid about a blunt body (within the framework of a thin shock layer analysis), the numerical computations presented in this report have been restricted to the stagnation region. Methods for iterating on the shock shape away from the stagnation region and typical results are available in Ref. 3. Our discussion here will consider only the methods for determining the stagnation point shock layer structure where we assume the shock wave is concentric to the body.

The computation flow logic is shown in Fig. 3. The input data prescribed are the stagnation-point radius of curvature (i.e., the characteristic body dimension), the body velocity and free stream density, and estimates of the shock layer thickness and enthalpy distribution.

The integral solution to the velocity field, i.e., the determination of the coefficients in Eq. (2.17) or Eqs. (2.18) and (2.19), is relatively straightforward although an iteration is required to solve the nonlinear algebraic equations involved. Note that the integral solution to the momentum equation, Eq. (2.9), requires thermodynamic and transport properties ($\rho\mu$) at the shock and wall. These are obtained using properties for air as originally correlated by Viegas and Howe (Ref. 11) and subsequently extended by Howe and Scheaffer (Ref. 12).

For problems with mass injection, $\dot{m} > 0$, the elemental specie diffusion equation, Eq. (2.37), is solved. Since a single diffusion coefficient is employed, the species within the ablation gases diffuse as a single entity and retain their relative concentration. Hence, only a single diffusion equation need be solved. The calculations presented in this report considered no surface reactions as it was found that surface reaction complicated the calculation but had only a minor effect on the net surface mass flux. For

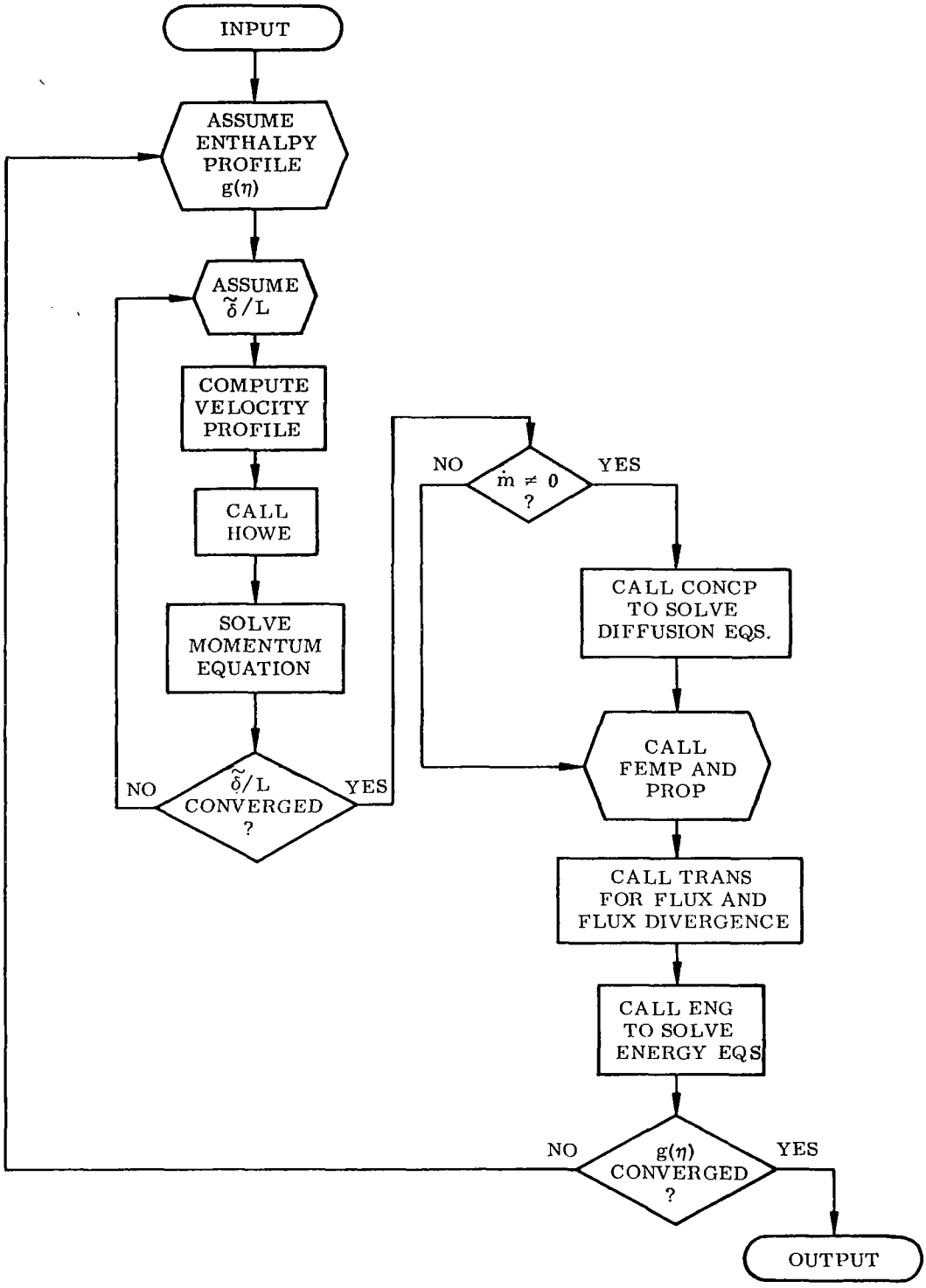

Fig. 3 Computational Flow Chart for VISC Code

the stagnation region and for no surface reactions, the solution to Eq. (2.37) can be obtained directly without iteration. After solution to the diffusion equation the detailed specie composition required for the radiation transport calculation is obtained from a detailed thermochemical code, FEMP. Details on the thermochemical calculation can be found in Ref. 4.

In preparation for numerical solution to the energy equation, the radiative flux divergence term E' is evaluated at selected points across the shock layer. Details on the radiative flux divergence calculation are given in Section 4. As expected, solution to the energy equation yielded the major source of numerical problems. The numerical problems resulted from the strong interaction between the radiant energy transport and the enthalpy distribution when the shock layer temperatures are large. This interaction was amplified under conditions of large mass injection. In order to prevent numerical instability we employed the following scheme in making successive approximations to the enthalpy profile: Let $g_a(\eta)$ be the previously assumed enthalpy profile used to calculate a new profile which we will call $g_b(\eta)$. Then the next estimate for continuing the energy equation iteration is a weighted average,

$$g_{guess}(\eta) = P\, g_b(\eta) + (1 - P)\, g_a(\eta)$$

For stability one expects $P < 1$ and to make any progress requires $P > 0$; hence, $0 < P < 1$. From experience it was found that $P \simeq 0.5$ led to a converged solution in a reasonable number of cycles. For problems without mass injection a reasonable input to the initial enthalpy distribution would lead to a converged solution. However, for large values of surface mass injection (say $\dot{m} \sim 0.1$) convergence was critically dependent upon the initial guess. Successful solution to the large mass injection problems required a background of knowledge obtained from previous lower $\dot{m}$ calculations.

It is of interest to note the convergence tolerance employed in our calculations. Earlier calculations used a 1% convergence of the enthalpy profile at

each selected η point. It was found, however, that while most of the enthalpy distribution would converge in a relatively small number of cycles, the solution would fail to converge at a few η points usually in the region of the steep enthalpy profile near the wall. By using a 5% tolerance it was found that most of the shock layer would converge to within 1% by the time the troublesome points converged to within 5%. As a result, a check showed that changing from 1% to 5% converged tolerance changed the radiative and convective heating rates by less than 1%. The calculations presented here were, for the most part, obtained using the 5% convergence factor.

Section 3
COUPLED, INVISCID RADIATING FLOWS

In this section we review a previously developed analysis (Ref. 13) of the flow of an inviscid, radiating gas past a blunt body with surface mass injection. By virtue of the inviscid model the injected, vaporized ablation-product gases are separated from the outer air flow by an interface. The momentum transfer from the outer air layer to the inner "vapor" layer is accomplished through the impressed streamwise pressure gradient at the interface. Transport of energy by radiation further couples the flow in these two separate layers.

3.1 GOVERNING EQUATIONS

The governing equations are developed here by expressing the conservation laws in terms of a boundary-layer type of coordinate system (Ref. 5). The air-vapor interface is introduced as the reference coordinate surface as this choice results in a degree of symmetry in the final equations describing the air and vapor regions. The geometric description of the coordinate system is shown in Fig. 4.

The conservation equations governing the shock layer flow field are as follows:

mass

$$\frac{\partial r'\rho'u'}{\partial x'} + \frac{\partial \tilde{K}r'\,\rho'v'}{\partial y'} = 0 \tag{3.1}$$

x-momentum

$$\rho'u'\frac{\partial u'}{\partial x'} + \tilde{K}\rho'v'\frac{\partial v'}{\partial y'} - k'\rho'u'v' + \frac{\partial P'}{\partial x'} = 0 \tag{3.2}$$

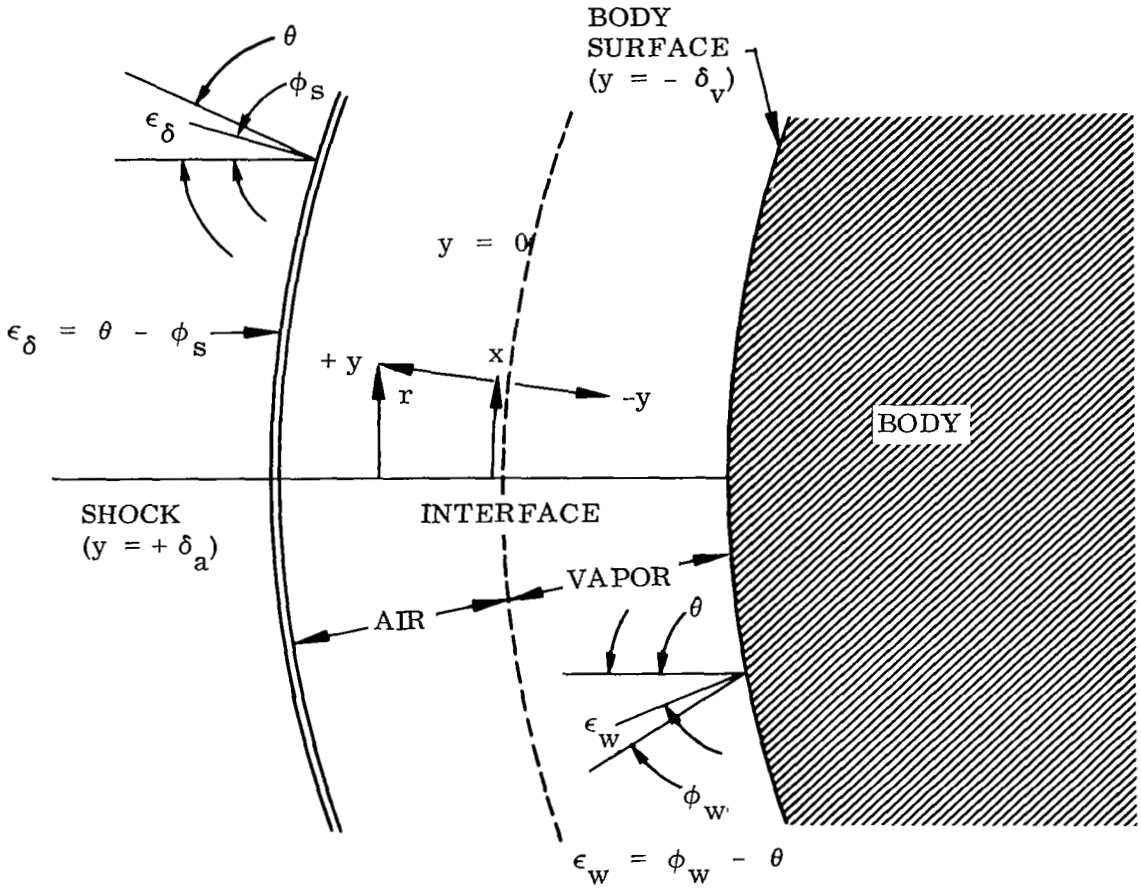

Fig. 4 Interface Oriented Coordinate System for Inviscid Analysis

y-momentum

$$\rho' u' \frac{\partial v'}{\partial x'} + \tilde{K}\rho' v' \frac{\partial v'}{\partial y'} - K'\rho' u'^2 + \tilde{K} \frac{\partial P'}{\partial y'} = 0 \tag{3.3}$$

energy

$$\rho' u' \frac{\partial H'}{\partial x} + \tilde{K}\rho' v' \frac{\partial H'}{\partial y'} + \tilde{K}\rho' E' = 0 \tag{3.4}$$

where

$$\tilde{K} = 1 + K'y' \tag{3.5}$$

The quantity E' appearing in the energy equation results from emission and absorption of radiation energy,

$$E' = \frac{1}{\rho'} \nabla \cdot \vec{F}' \tag{3.6}$$

where F is the radiative flux vector.

The order of the shock layer thickness and normal velocity component is $O(\bar{\rho})$, where $\bar{\rho}$ is the density ratio across the shock ($\bar{\rho} = \rho'_\infty/\rho'_\delta$). Then introducing the following nondimensional forms, all quantities become of $O(1)$,

$$u = \frac{u'}{U'_\infty} \qquad v = \frac{v'}{\bar{\rho} U'_\infty} \qquad \rho = \frac{\rho'}{\rho'_\delta} \qquad p = \frac{p'}{\rho'_\infty U'^2_\infty}$$

$$x = \frac{x'}{R'} \qquad y = \frac{y'}{\bar{\rho} R'} \qquad K = \frac{K'}{R'} \qquad r = \frac{r'}{R'}$$

$$H = \frac{2H'}{U'^2_\infty}$$

Then the conservation equations become

$$\frac{\partial r\rho u}{\partial x} + \frac{\partial}{\partial y}\,\tilde{K} r\rho v = 0 \tag{3.7}$$

$$\rho u \frac{\partial u}{\partial x} + \tilde{K}\rho v \frac{\partial u}{\partial y} + \bar{\rho} K \rho u v - \bar{\rho} \frac{\partial P}{\partial x} = 0 \tag{3.8}$$

$$- K\rho u^2 + \tilde{K} \frac{\partial p}{\partial y} = 0 \tag{3.9}$$

$$\rho u \frac{\partial H}{\partial x} + \tilde{K}\rho v \frac{\partial H}{\partial y} + \alpha_o \tilde{K}\rho E' = 0 \tag{3.10}$$

where

$$\alpha_o = \frac{2L}{U_\infty^3}$$

$$\tilde{K} = 1 + \bar{\rho} K y$$

In the y-momentum equation, terms of $O(\bar{\rho})$ have been neglected since the entire y-momentum equation will be multiplied by $\bar{\rho}$ in combining it with the x-momentum equation. Hence the $\bar{\rho}$ terms in the y-momentum equation will be of higher order in determining the momentum flux in the x-direction.

3.2 VELOCITY FIELD SOLUTION

These conservation equations apply, of course, in both the air and vapor regions. We now treat the air and vapor regions separately. The two momentum equations are combined and, together with the mass equation, are integrated across the air and vapor layers independently to determine the mass and x-momentum flux in each region (cf. Ref. 13 for further detail). The results are as follows:

Air layer

$$\frac{dI_{a,0}}{dx} + I_{a,0}\frac{d}{dx}\ln(r_v u_\delta) - \frac{1}{\rho_\delta u_\delta}\left(\frac{r_s}{r_v}\right)\left[\frac{d\delta_a}{dx} - \tilde{K}_\delta \frac{v_\delta}{u_\delta}\right] = 0 \tag{3.11}$$

$$\frac{dI_{a,1}}{dx} + I_{a,1}\, d\ln(r_v u_\delta^2) - \bar{\rho}\frac{dK}{dx} I_{a,2} - \frac{\tilde{K}_\delta}{\rho_\delta u_\delta}\left(\frac{r_s}{r_v}\right)\left[\frac{d\delta_a}{dx} - \frac{\tilde{K}_s v_\delta}{u_\delta}\right] + \frac{\bar{\rho}\delta_a}{\rho_\delta u_\delta^2}\left(\frac{\partial P}{\partial x}\right)_{y=\delta_a} = 0 \tag{3.12}$$

where

$$I_{a,0} = \int_0^{\delta_a}\left(\frac{r}{r_v}\right)\left(\frac{\rho}{\rho_\delta}\right)\left(\frac{u}{u_\delta}\right) dy \tag{3.13}$$

$$I_{a,1} = \int_0^{\delta_a}\left(\frac{r}{r_v}\right)\left(\frac{\rho}{\rho_\delta}\right)\left(\frac{u}{u_\delta}\right)^2 dy \tag{3.14}$$

$$I_{a,2} = \int_0^{\delta_a} y\left(\frac{r}{r_v}\right)\left(\frac{\rho}{\rho_\delta}\right)\left(\frac{u}{u_\delta}\right)^2 dy \tag{3.15}$$

Vapor layer

$$\frac{dI_{v,0}}{dx} + I_{v,0}\frac{d}{dx}\ln(r_v\rho_w u_v) - \left(\frac{r_w}{r_v}\right)\frac{\dot{m}\, u_w}{\rho_w u_v v_w}\left[\frac{d(-\delta_v)}{dx} - \frac{\tilde{K}_w v_w}{u_w}\right] = 0 \tag{3.16}$$

$$\frac{dI_{v,1}}{dx} + I_{v,1}\frac{d}{dx}\ln(r_v\rho_w u_v^2) + \bar{\rho}K\left[\frac{dI_{v,1}}{dx}\ln K + \left(\frac{d\ln r_v}{dx}\right) I_{v,2}\right] - \left(\frac{r_w}{r_v}\right)\frac{\dot{m}\, u_w^2}{\rho_w v_w u_v^2}\left[\frac{d(-\delta_v)}{dx} - \frac{K_w v_w}{u_w}\right] - \frac{\bar{\rho}\,\delta_v}{\tilde{K}_w\rho_w u_v^2}\left(\frac{\partial P}{\partial y}\right)_{y=0} = 0 \tag{3.17}$$

where

$$I_{v,0} = \int_0^{-\delta_v} \left(\frac{r}{r_v}\right) \frac{\rho}{\rho_w} \frac{u}{u_v}\, dy \tag{3.18}$$

$$I_{v,1} = \int_0^{-\delta_v} \left(\frac{r}{r_v}\right)\left(\frac{\rho}{\rho_w}\right)\left(\frac{u}{u_v}\right)^2 dy \tag{3.19}$$

$$I_{v,2} = \int_0^{-\delta_v} y \left(\frac{r}{r_v}\right)\left(\frac{\rho}{\rho_w}\right)\left(\frac{u}{u_v}\right)^2 dy \tag{3.20}$$

The integrals $I_{a,0}$ and $I_{v,0}$ represent the flux mass though the air and vapor layers, respectively. The integrals $I_{a,1}$ and $I_{v,1}$ represent the flux of momentum in the x-direction through the air and vapor layers, respectively. The integrals $I_{a,2}$ and $I_{v,2}$ represent a weighted momentum flux and have no particular physical significance. Indeed, since $I_{a,2}$ and $I_{y,2}$ are multiplied by $\bar{\rho}$ (i.e., these integral terms represent a small effect in the x-momentum equations) then it will be sufficient to approximate $I_{a,2}$ and $I_{v,2}$ in terms of $I_{a,1}$ and $I_{v,1}$.

The determination of the flow field requires the solution of the above differential equations for the flux integrals. For the air region, the system of equations is linear and can be reduced to a quadrature. In the vapor layer equations the velocity at the vapor side of the interface u_v is a basic unknown together with the integrals $I_{a,v}$ and $I_{l,v}$. There exist algebraic equations coupling u_v with these integrals as derived from Eqs. (3.18) and (3.19). By appropriate manipulation, the vapor equations can be reduced to a single equation in u_v, as will be shown later.

Consider next the determination of the tangential velocity distribution and shock layer thickness in terms of the calculated mass and momentum flux integrals. It is convenient to describe the flow field in terms of a transformed normal coordinate in which the effects of geometry and the density variation are reduced. This effectively uncouples the flow field solution from the energy equation. Define for the air region

$$\eta = \frac{\int_o^y (\frac{r}{r_v})(\frac{\rho}{\rho_\delta})\, dy'}{\tilde{\delta}_a} \tag{3.21a}$$

$$\tilde{\delta}_a = \int_o^{\delta_a} (\frac{r}{r_v})(\frac{\rho}{\rho_\delta})\, dy' \tag{3.21b}$$

and for the vapor region

$$\eta = - \frac{\int_o^y (\frac{r}{r_v})(\frac{\rho}{\rho_w})\, dy'}{\tilde{\delta}_v} \tag{3.22a}$$

$$\tilde{\delta}_v = \int_o^{-\delta_v} (\frac{r}{r_v})(\frac{\rho}{\rho_w})\, dy' \tag{3.22b}$$

The flux integrals for the air layer become

$$I_{a,0} = \tilde{\delta}_a \int_o^1 (\frac{u}{u_\delta})\, d\eta \tag{3.23}$$

$$I_{a,1} = \tilde{\delta}_a \int_o^1 (\frac{u}{u_\delta})^2\, d\eta \tag{3.24}$$

Equations (3.23) and (3.24) determine the transformed air layer thickness and the tangential velocity field in an integral sense. Hence if we specify a velocity distribution in terms of a single free parameter (x-dependent), then the coupled equation ((3.23) and (3.24)) determine $\tilde{\delta}_a(x)$ and this free parameter.

In terms of the η coordinate, it has been found that the tangential velocity

field can be well approximated by a linear distribution (Ref. 13)

$$\frac{u}{u_\delta} = a_0 + a_1 \eta \tag{3.25}$$

This distribution is subject to the boundary condition

$$\frac{u}{u_\delta} = 1 \quad @ \ \eta = 1 \tag{3.26}$$

which reduces the velocity distribution to

$$\frac{u}{u_\delta} = a_0 + (1 - a_0)\ \eta \tag{3.27}$$

where a_0 is the desired free parameter.

The flux integrals for the vapor layer become

$$I_{v,0} = - \tilde{\delta}_v \int_0^1 \left(\frac{u}{u_v}\right) d\eta \tag{3.28}$$

$$I_{v,1} = - \tilde{\delta}_v \int_0^1 \left(\frac{u}{u_v}\right)^2 d\eta \tag{3.29}$$

Work on constant density vapor layer flows has shown the tangential velocity distribution to be linear in the physical coordinate y (Ref. 13). Since the transformation to the η coordinate removes variable density effects, then it is reasonable to assume a linear velocity field,

$$\frac{u}{u_v} = b_0 + b_1\eta \tag{3.30}$$

This distribution is subject to the boundary condition

$$\frac{u}{u_v} = 1 \quad \text{at} \quad \eta = 0 \tag{3.31}$$

so that $b_0 = 1$.

The velocity at the body surface is also prescribed by the assumption of normal (to body) injection at a rate $\dot{m}$. Hence at the body surface

$$\frac{u}{u_v} = \frac{u_w}{u_v} \qquad @\ \eta = 1 \tag{3.32}$$

so that b_1 is known if we consider u_v fixed. In fact, when the interface is concentric with the body b_1 is identically zero. Hence, Eq. (3.30) has no free parameter. This does not mean, however, that the solution to the velocity field has been overdetermined. The integrals $I_{v,0}$ and $I_{v,1}$ reduce to a single unknown $\tilde{\delta}_v$ but the variable u_v is also unknown. Hence, Eq. (3.16 and (3.17) reduce to a set of coupled equations in $\tilde{\delta}_v$ and u_v. In terms of these variables, Eqs. (3.16) and (3.17) can be reduced to the following equation for u_v (Ref. 13)

$$\frac{du_v}{dx} + u_v\left[\frac{d\ \ln}{dx}\left(\frac{r_v}{K}\right)^{\beta_v} + \frac{\tilde{K}_w\, r_w\, \dot{m}}{S\cos\epsilon_w}\right] - \frac{3}{2}\left[\tilde{K}_w\, r_w\, \dot{m}\left(\frac{\dot{m}}{\rho_w}\right)\tan\epsilon_w\right.$$

$$\left. - \frac{\bar{\rho}\,\delta_v\, r_w}{\tilde{K}_w}\ \frac{dp_v}{dx}\right] = 0 \tag{3.33}$$

where

$$S = \int_0^x \frac{\tilde{K}_w \, r_w \, \dot{m}}{\cos \epsilon_w} \, dx$$

$$\beta_v = \frac{\bar{\rho} \, K \, \delta_v}{2}$$

In deriving Eq. (3.33) the following relation was employed:

$$\left[\frac{d(-\delta_v)}{dx} - \frac{\tilde{K}_w \, v_w}{u_w}\right] = - \frac{\tilde{K}_w \, \dot{m}}{\rho_w u_w} \tan \epsilon_w$$

The transformed shock layer thickness follows from the integrated mass conservation equation,

$$\tilde{\delta}_v = - \frac{2S}{\left(1 + \frac{u_w}{u_v}\right) r_v \, \rho_w \, u_v} \qquad (3.34)$$

Using the calculated velocity distribution, the pressure distribution in the entire shock layer can be determined from Eq. (3.9), transformed to η, x coordinates. This completes the flow field solution. In order to express the solution in physical coordinates the energy equation must be solved for the enthalpy and density distributions.

3.3 ENERGY EQUATION SOLUTION

The energy equation is solved exactly in terms of a detailed numerical integration through the shock layer. The solution follows the method of Smith and Clutter (Ref. 6) developed for nonsimilar boundary layer problems. Transformation is made first to η,x coordinates. The stream function ψ satisfies the following relations:

$$r\rho u = -\left.\frac{\partial \psi}{\partial y}\right)_x \tag{3.35a}$$

$$\tilde{K} r\rho v = \left.\frac{\partial \psi}{\partial x}\right)_y \tag{3.35b}$$

In the air layer, a normalized stream function is defined as

$$f_a = \frac{\psi}{r_\delta \rho_\delta u_\delta} \tag{3.36}$$

whereupon the energy equation takes the form (we define $g = H/H_\delta$ noting that H_δ = constant)

$$\left[u_\delta \left(\frac{\partial f_a}{\partial \xi}\right) + f_a \left(\Gamma_a + \Omega_a\right)\right] \frac{dg_a}{d\eta} = \left[u_\delta f_a' \left(\frac{\partial g_a}{\partial x}\right) - \tilde{\delta}_a \alpha_o \tilde{K} E'\right] \tag{3.37}$$

$$\Gamma_a = \frac{du_\delta}{dx} \tag{3.38}$$

$$\Omega_a = \frac{u_\delta}{r_v} \frac{dr_v}{dx} \tag{3.39}$$

$$f_a' = \left.\frac{\partial f_a}{\partial \eta}\right)_x \tag{3.40}$$

The functions Γ_a and Ω_a are directly available from the shock boundary conditions and the interface description. In terms of Eq. (3.35a) and the η, x transformation equations it can be shown that

$$f_a' = \tilde{\delta}_a \left(\frac{u}{u_\delta}\right) \tag{3.41}$$

Integrating Eq. (3.41) and applying the boundary condition,

$$f_a(x) = 0 \quad \text{at} \quad \eta = 0 \tag{3.42}$$

yields the required relation for $f_a(x)$.

An analogous equation is derived for the vapor layer

$$\left[u_v \left(\frac{\partial f_v}{\partial \xi}\right)_\eta + f_v \left(\Gamma_v + \Omega_v\right)\right] \frac{dg_v}{d\eta} = \left[u_v f_v' \left(\frac{\partial g_v}{\partial \xi}\right)_\eta + \tilde{\delta}\, \alpha_o K E'\right] \tag{3.43}$$

where

$$\Gamma_v = \frac{du_v}{dx} \tag{3.44}$$

$$\Omega_v = \frac{u_v}{r_v} \frac{dr_v}{dx} \tag{3.45}$$

$$f_v' = \frac{\partial f_v}{\partial \eta}\, x \tag{3.46}$$

The normalized stream function f_v is defined by

$$f_v = \frac{\psi}{r_v \rho_w u_v} \tag{3.47}$$

so that

$$f_v' = \tilde{\delta}_v \frac{u}{u_v} \tag{3.48}$$

which is subject to the boundary condition

$$f_v(x) = 0 \quad @ \quad \eta = 0 \tag{3.49}$$

Equations (3.37) and (3.43) are integrated at various points about the body (i.e., along lines x = constant). The x-wise derivatives

$$\left(\frac{\partial g}{\partial x}\right)_\eta \quad \text{and} \quad \left(\frac{\partial f}{\partial x}\right)_\eta$$

are evaluated from backwards difference equations. This is consistent with the parabolic nature of the original set of partial differential equations. Since Eqs. (3.37) and (3.43) are first order, only one initial value is needed in the air and vapor regions. These initial conditions are

$$@ \quad \eta = 1 \qquad g_a = 1 \tag{3.50}$$

$$@ \quad \eta = -1 \qquad g_v = g_w \tag{3.51}$$

where the wall enthalpy g_w is specified.

The air layer energy equation is integrated from the shock ($\eta = 1$) to the interface ($\eta = 0$) while the vapor layer energy equation is integrated from the body surface ($\eta = -1$) to the interface ($\eta = 0$).

The radiation flux divergence term is calculated assuming the shock layer to be locally one-dimensional. The radiation flux and flux divergence expressions are developed in Section 4.*

*The general radiative transport solution developed in Section 4 includes both continuum and line transport. However, for the inviscid analysis, only the continuum transport term was included in E'.

3.4 NUMERICAL METHODS

As in the viscous analysis of Section 2, the numerical methods separate into two distinct parts. One part is the determination of the shock wave and interface shape (assuming a given mass injection distribution along the surface) and the other part is the determination of the shock layer flow field structure in both the air and vapor regions. Although the analysis presented above is applicable about a blunt body (within the framework of a thin shock layer analysis) the numerical computations presented in this report are limited to the stagnation region. Our discussions in this section are therefore limited to methods for determining the stagnation region shock layer structure under the assumption of a concentric shock wave-interface-body.

The solution to the momentum equations is relatively straightforward. Limiting forms of Eqs. (3.11) and (3.12) are obtained under the condition $dI_{a,0}/dx = dI_{a,1}/dx = 0$. The resulting solutions for $I_{a,0}$ and $I_{a,1}$ are combined with Eqs. (3.23) and (3.24) to determine $\tilde{\delta}_a$ and a_0. For the vapor region (where the concentric interface assumption yields $u_w = 0$ and $\epsilon_w = 0$), Eq. (3.33) can be integrated in terms of the limiting form of $S(x)$ and the expression for $dp_v/dx = dp_a/dx$ obtained from the x-momentum equation evaluated in the air layer at $\eta = 0$. This solution to Eq. (3.33) determines u_v which allows $\tilde{\delta}_v$ to be calculated from Eq. (3.34).

The solution to the energy equation is obtained by integrating the first order equations, Eq. (3.37), in the air layer and Eq. (3.43) in the vapor layer. At the stagnation point the terms $\partial g_a/\partial\xi$, $\partial f_a/\partial\xi$ $\partial g_v/\partial\xi$, and $\partial f_v/\partial\xi$ are all zero. As one expects, numerical problems are encountered when the temperature in the air layer is large. Under these conditions the strong dependence of the radiative flux divergence on the enthalpy levels makes the numerical integrations quite unstable. The scheme discussed in Section 2.5 for using a weighted average of the enthalpy distribution in proceeding from one iteration to the next was employed in the inviscid calculations. A further difficulty is encountered at the point $\eta = 0$ for which the energy equation in both the air and vapor region becomes singular. Physically, we have a situation in

which, under the inviscid model, the gas approaches radiative equilibrium ($E' \rightarrow 0$) as the normal velocity approaches zero at the interface. This difficulty was circumvented by the expediency of limiting the numerical integration to a value $|\eta^*| > 0$. Typically, we set $|\eta^*| = 0.01$. Since the enthalpy and pressure distributions were usually "flat" near $\eta = 0$, we could then extrapolate the values of $g_a(\eta^*)$ and $g_v(\eta^*)$ to $\eta = 0$. The convergence tolerance employed in the inviscid analysis was the same value of 5% used in the viscous analysis. The argument set forth in Section 2.5 for the validity of a 5% convergence criteria holds for the inviscid problem.

Section 4
RADIATION TRANSPORT

We consider in this section the radiative flux F' and the flux divergence E' which appear in the energy equation in both the viscous (Section 2) and inviscid (Section 3) analysis of radiating flows. Transport expressions are derived for a one-dimensional planar geometry with the gas in local thermodynamic equilibrium. Primary emphasis is placed on the handling of discrete (i.e., line) absorption processes in the transport equation. The importance of atomic lines is now well recognized as a result of earlier investigations (Refs. 14, 15) of radiative transport in plasmas. Transport due to continuous absorption processes, including molecular line transitions treated by the usual band model, is included.

4.1 Basic Transport Equations

The flux and flux divergence are given by

$$F'(y) = \int_0^\infty \int_{\omega=4\pi} I(y,\nu,\omega)\, d\omega\, d\nu \tag{4.1}$$

and

$$\nabla\cdot F'(y) = \int_0^\infty \int_{\omega=4\pi} \mu(y,\nu) \left[I(y,\nu,\omega) - B(y,\nu) \right] d\omega\, d\nu \tag{4.2}$$

where $I(y,\nu,\omega)$ is the monochromatic intensity at frequency ν and in the direction ω. The angular integration in Eqs. (4.1) and (4.2) is carried out using the forward-reverse approximation due to Schwartzchild (Ref. 16). The intensity is divided into two angular groups: those rays passing in the positive direction from left-to-right through a plane of symmetry (i.e., a plane normal to the y axis in our one-dimensional planar geometry) and those rays passing in a negative direction from right-to-left. The forward-reverse

approximation represents all rays in the positive direction by a single ray I^+ with an average direction cosine $1/\ell$ and all rays in the negative direction by a single ray I^- also with an average direction cosine $1/\ell$ (cf. Fig. 5)

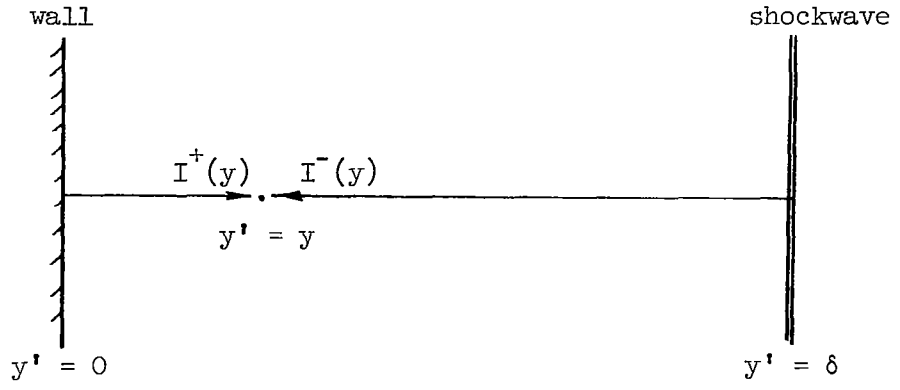

Figure 5 Geometry for Radiative Transport in a One-dimensional Planar Medium

As is well known, this two-stream approximation is equivalent to the exponential approximation to the exponential integral kernel function which arises in an exact formulation. An analysis of transport in a uniform gas (Ref. 17) shows that a value of $\ell = 2$ provides a good approximation to the exact flux and flux divergence values.

The monochromatic intensities I^+ and I^- are given by

$$I^+(\nu,y) = \int_0^y \mu(\nu,y')\, B(\nu,y')\, e^{-\ell\int_{y'}^{y} \mu(\nu,y'')\, dy''}\, dy' \qquad (4.3a)$$

$$I^-(\nu,y) = \int_y^\delta \mu(\nu,y')\, B(\nu,y')\, e^{-\ell\int_{y}^{y'} \mu(\nu,y'')\, dy''} \qquad (4.3b)$$

In carrying out the frequency integration in Eqs. (4.1) and (4.2), the absorption coefficient is separated into the continuum and line contribution.

$$\mu(\nu,y') = \mu^C(\nu,y) + \mu^L(\nu,y) \tag{4.4}$$

The flux may then be expressed as the sum of a contribution due to continuum only processes F^C and a contribution due to lines but corrected for continuum attenuation.

$$F(y) = F^C(y) + F^L(y) \tag{4.5}$$

For the continuum contribution we evaluate monochromatic values at selected frequencies, and then perform a numerical quadrature over frequency.

$$F^C(y) = \pi \int_o^\infty \left\{ \int_o^{E(o,y)} B(\nu,y')\, dE_\nu(y',y) - \int_o^{E(y,\delta)} B(\nu,y')\, dE_\nu(y,y') \right\} d\nu \tag{4.6}$$

where the emissive function $E_\nu(y,y')$ is introduced to simplify the numerical spatial integrations,

$$E_\nu(y',y) = E_\nu\left[-(y,y')\right] = 1 - \exp\left[-\ell \int_{y'}^{y} \mu^C(\nu,y'')\, dy''\right] \tag{4.7}$$

For the line contribution, the integration over frequency is carried out analytically for individual or groups of individual lines and the total contribution summed over all lines or groups of lines,

$$F^L(y) = \pi \sum_{\text{all lines } i} \left\{ \int_o^{W_i(o,y)} B_i(y')\, dW_i(y',y) - \int_o^{W_i(y,\delta)} B_i(y')\, dW(y,y') \right\} \tag{4.8}$$

where the frequency integration performed in terms of an equivalent width variable $W_i(y',y)$ defined as

$$W_i(y',y) = W_i\left[-(y,y')\right] = e^{-\ell\int_{y'}^{y}\mu_i^C(y'')dy''} \int_{\Delta\nu}\left[1-\exp(-\ell\int_{y'}^{y}\mu_i^L(\nu,y'')\,dy'')\right]d\nu \tag{4.11}$$

In defining $W_i(y',y)$ in this manner we have assumed that the Planck function and continuum absorption are frequency independent (at least approximately) over the interval $\Delta\nu$.

In a similar manner, we treat the flux divergence as due to a continuum only contribution and terms due to lines plus continuum. Due to cross terms there are a total of four contributions (Ref. 17).

$$E' = \nabla\cdot F' = Q^{C,C}(y) + Q^{C,L}(y) + Q^{L,C}(y) + Q^{L,L}(y) \tag{4.12}$$

These Q terms are defined as:

(1) the energy emitted and absorbed by the continuum;

$$Q^{C,C}(y) = 2\pi\int_0^\infty \mu^C(y)\left\{\int_0^{E_\nu(o,y)} B(\nu,y')\,dE_\nu(y,y') + \int^{E_\nu(y,\delta)} B(\nu,y')\,dE_\nu(y',y) - 2B(\nu,y)\right\}d\nu \tag{4.13}$$

(2) the energy emitted by the continuum and absorbed by the lines;

$$Q^{C,L} = 2\pi\sum_{\text{all lines, i}}\left\{\int_0^{E_\nu(o,y)} B_i(y')\left[S_i(y) - A_i(y,y')\right]dE_\nu(y',y) + \int_0^{E_\nu(y,\delta)} B_i(y')\left[S_i(y) - A_i(y,y')\right]dE_\nu(y,y')\right\} \tag{4.14}$$

(3) the energy emitted by lines and absorbed by the continuum;

$$Q^{L,C} = 2\pi \sum_{\text{all lines},i} \mu_i^C(y) \left\{ \int_o^{W_i(o,y)} B_i(y')\, dW_i(y',y) + \int_o^{W_i(y,\delta)} B_i(y')\, dW_i(y,y') \right\} \tag{4.15}$$

(4) the energy absorbed and emitted by lines,

$$Q^{L,L} = 2\pi \sum_{\text{all lines},i} \int_o^{A_i(o,y)} B_i(y')\, e^{-\ell\int_{y'}^{y} \mu_i^C(d'')dy''}\, dA_i(y',y) + \int_o^{A_i(y,\delta)} B_i(y')\, e^{-\ell\int_{y}^{y'} \mu_i^C(y'')dy''}\, dA_i(y,y') - 2B_{\nu_i}(y) \tag{4.16}$$

In eqs. (4.14) and (4.16) the frequency integration is performed in terms of an absorption equivalent width variable $A_i(y',y)$ defined as

$$A_i(y',y) = A_i\left[-(y,y')\right] = \int_{\Delta\nu} \mu_i^L(\nu,y)\left[1-\exp(-\ell \sum_i \int_{y'}^{y'} \mu_i^L(\nu,y'')dy'')\right] d\nu \tag{4.17}$$

The continuous spectral absorption processes considered are the free-free and bound-free transitions of H, C, C^+, N, N^+, O, O^+ atoms and the molecular band systems given in Table A-I, Appendix A. Detailed equations for the atomic and molecular continuum absorption coefficients are given in Appendix A.

We will discuss the evaluation of the line contribution to the flux and flux divergence first in terms of a single isolated line. The problem of overlapping ing of closely spaced lines will be handled later. For the plasmas of interest an isolated line has a Lorentzian shape characterized by a strength S and (half) half-width determined by electron impact,*

$$\mu_i^L(\nu) = \frac{S_i \gamma_i}{\pi} \frac{1}{(\nu-\nu_i)^2+\gamma_i^2} \tag{4.18}$$

where

$$S_i \equiv \int_{\Delta\nu} \mu_i^L(\nu)\, d\nu = \frac{\pi e^2}{mc} N_i f_i \tag{4.19}$$

where N_i is the number density of the lower state and f_i the f-number determining the transition probability strength. In our calculations of the line transport we have used the tabulation of Wilson and Nicolet (Ref. 18) of γ_i and f_i for neutral and ionized carbon, nitrogen, and oxygen atoms. We have omitted hydrogen lines since they are non-Lorentzian in shape and are estimated to have only a small effect in terms of total radiative transport.

Then for a Lorentzian shape and assuming an isolated line, the frequency integration over the line required in the definitions of W_i, Eq. (4.11) and A_i, Eq. (4.17), can be carried out exactly. We will use, however, the limiting forms for these frequency integrals valid for optically thin or optically thick gases (Ref. 17). Define the optical depth at the line center,

$$\tau_i = \ell \left| \int_y^{y'} \frac{S_i}{\pi \gamma_i}\, dy'' \right| \tag{4.20}$$

*In general, $\mu_i^L(\nu)$ should include, in the denominator of Eq. (4.18), a line center shift. This shift, however, can be neglected in treating transport problems.

Then for $\tau_i \leq 4/\pi$

$$W_i(y,y') = e^{-\ell\int_{y'}^{y} \mu_{\nu_i}^{C}(y'')dy''} \left[\left|\int_{y'}^{y} S(y'')dy''\right|\right] \tag{4.21}$$

$$A_i(y,y') = \left[\frac{S_i}{\pi\,\gamma_i}\left|\int_{y'}^{y} \frac{S_i(y'')}{\pi\left(\frac{\gamma_i(y'')}{\gamma_i(y)} + 1\right)}\,dy''\right|\right] \tag{4.22}$$

For $\tau_i > 4/\pi$

$$W_i(y,y') = 2e^{-\ell\int_{y'}^{y} \mu_i^{C}(y'')dy''} \left[\left|\int_{y'}^{y} S_i(y'')\,\gamma_i(y'')\,dy''\right|\right]^{1/2} \tag{4.23}$$

$$A_i(y,y') = S_i\left[1 - e^{-g(y,y')}\left(1 - \Phi\sqrt{g(y,y')}\right)\right] \tag{4.24}$$

where

$$g = \frac{1}{\pi}\left|\int_{y'}^{y} \frac{S_i(y'')\,\gamma_i(y'')}{\gamma_i^{2}(y)}\,dy''\right| \tag{4.25}$$

and Φ is the error integral.

So far we have considered only a single isolated line. We will now develop an approximate model to handle the multitude of line transitions in a plasma of C, N, and O atoms. In developing this model we will consider at first only a nitrogen plasma. However, the resultant model is felt to be general and applicable to a collection of C, N, and O atoms.

As a "standard" for comparing our approximate model, solutions for both the flux and flux divergence were obtained considering the individual contributions of roughly 100 nitrogen lines divided into 18 groups (Ref. 17). Within each group (typically covering a spectral interval of about $\Delta h\nu = 1$ eV) we assume the Planck function B_i and continuum absorption coefficient μ_i^C to be constant in frequency. This group method reduces somewhat the number of spatial integrations required but the solution is essentially an exact line-by-line calculation.

The accounting of many lines in a coupled flow problem is quite time-consuming. Thus we were motivated to develop an "equivalent line" model in which each line group is characterized by a single, averaged f-number and half-width. The averaging scheme was derived in terms of the flux and flux divergence expressions for an homogeneous plasma. The validity of this approach lies in a comparison of the results obtained using the approximate model with those obtained for the line-by-line calculation.

For an homogeneous plasma Eq. (4.14) for the one-sided flux reduces to

$$F^+ = \pi B W_{line} \tag{4.26}$$

where W_{line} is the width of an "equivalent" line. For optically thin lines

$$W_{line} = C_o \delta \sum_{i=1}^{n} (N_i f_i) \tag{4.27}$$

where $C_o = \pi e^2/mc$. We define an equivalent f-number $\bar{f}$ such that

$$W_{line} = n\, C_o \delta\, N\, \bar{f} \tag{4.28}$$

where n is the number of lines under consideration and N is the total number density of the absorbing atoms (in this case nitrogen only). Then

$$\bar{f} = \frac{1}{n} \sum_{i=1}^{i=n} \left(\frac{N_i}{N} f_i\right) \tag{4.29}$$

For optically thick lines

$$W_{line} = 2 \sqrt{C_o \delta} \sum_{i=1}^{n} (N_i f_i \gamma_i)^{1/2} \tag{4.30}$$

and we define an equivalent half-width $\bar{\gamma}$ such that

$$W_{line} = 2 \sqrt{C_o \delta}\ n\ (N \bar{f} \bar{\gamma})^{1/2} \tag{4.31}$$

then

$$\bar{\gamma} = \frac{1}{n^2 \bar{f}} \left\{ \sum_i \left(\frac{N_i}{N} f_i \gamma_i\right)^{1/2} \right\}^2 \tag{4.32}$$

For an homogeneous plasma Eq. (4.16) for the line contribution to the flux divergence reduces to

$$Q^{LL} = 2\pi B \left[A^{+}_{line} + A^{-}_{line} - 2S_{line}\right] \tag{4.33}$$

where A_{line} is the absorption width of an "equivalent" line. Since

$$S_{line} = C_o \sum_{i=1}^{n} (N_i f_i) \tag{4.34}$$

then we can use the previously defined equivalent f-number to obtain

$$S_{line} = n\, C_o (N\, \bar{f}) \tag{4.35}$$

For the absorption weighted equivalent width, in the thin limit

$$A^{+}_{line} = \frac{\delta}{\pi^2} C_o^2 \sum_{i=1}^{n} \left(\frac{N_i f_i^2}{\gamma_i} \right) \tag{4.36}$$

and we define an absorption half-width $\bar{\alpha}$ for the thin case such that

$$A^{+}_{line} = n \frac{\delta}{\pi^2} C_o^2 \frac{N\, \bar{f}^2}{\bar{\alpha}} \tag{4.37}$$

Then

$$\bar{\alpha} = \frac{n\, \bar{f}^2}{\sum_{i=1}^{n} \left(\frac{N_i}{N} \frac{f_i^2}{\gamma_i} \right)} \tag{4.38}$$

For the absorption weighted equivalent width, in the thick limit we use the limiting form for A_{ν_o} valid when $g = \tau_i \gg 1$,

$$A = C_o \sum_i N_i f_i \left\{ 1 - \frac{1}{\left(\frac{C_o N_i f_i \delta}{\gamma_i} \right)^{1/2}} \right\} \tag{4.39}$$

and we define an absorption half-width $\bar{\beta}$ for the thick case such that

$$A = n C_o N \bar{f} \left\{ 1 - \frac{1}{\left(\frac{C_o N \bar{f} \delta}{\bar{\beta}} \right)^{1/2}} \right\} \tag{4.40}$$

then

$$\bar{\beta} = \frac{1}{n^2 \bar{f}} \left\{ \sum_i \left(\frac{N_i}{N} f_i \gamma_i \right)^{1/2} \right\}^2 \tag{4.41}$$

But Eq. (4.41) is identical to Eq. (4.32), i.e., $\bar{\beta} \equiv \bar{\gamma}$ so that the width parameter used to calculate the flux from a set of optically thick lines can also be used to calculate the flux divergence.

Using Eqs. (4.29), (4.32), and (4.38) values of $\bar{f}$, $\bar{\gamma}$, and $\bar{\alpha}$ were calculated for five equivalent lines approximating a nitrogen plasma. The spectral location, spectral interval, and number of weighted lines characterized by each equivalent line are shown in Table I, below. The actual $\bar{f}$, $\bar{\gamma}$, and $\bar{\alpha}$ values are temperature dependent and hence depend on the specific plasma conditions.

TABLE I Equivalent Line Properties
(Nitrogen Plasma)

Equivalent Line No., k	Spectral Location, $h\nu_k$	Spectral Interval, D_k	Number of Lines, n_k
1	1.20 eV	1.43 eV	14
2	3.40 eV	1.60 eV	7
3	8.60 eV	3.50 eV	6
4	10.40 eV	1.10 eV	9
5	11.50 eV	1.20 eV	10

We address ourselves now to the general problem of overlapping. To account for overlapping, we calculate an isolated line equivalent width, W_I and then borrow from Plass (Ref. 19) the following expression for the width of a collection of overlapping lines under the statistical model.

$$\frac{W_{line}}{D} = \left[1 - e^{-(W_I/d)}\right] \tag{4.42}$$

where D is the spectral interval covered by the equivalent line and d is the line spacing within that interval, $d = D/n$. Rather than attempting to rationalize Eq. (4.42) in terms of the number of actual lines represented by each equivalent line (cf. Table II), we simply accept Eq. (4.42) as an empirical relation valid when $W_I/d \ll 1$ and $W_I/d \gg 1$. Numerical calculations show that the error introduced in Eq. (4.42) is largest roughly when $W_I/d \sim 0.5$ and the level of error is an under estimate of W_{line} of about 25%.

In a similar manner, one can argue heuristically that when line overlapping becomes very large the value of the absorption width A_{line} appearing in the flux divergence expression (cf. Eq. (4.17)) asymptotically approaches S_{line}. The rate of approach to this asymptotic limit is measured by W_I/d. Then we propose the empirical interpolation relation

$$A_{line} = S_{line} - \left(\frac{1}{1 + W_I/d}\right)(S_{line} - A_I) \tag{4.43}$$

where A_I is calculated assuming an isolated line model. Using Eq. (4.43), A_{line} approaches A_I when $W_I/d \ll 1$ and approaches S_{line} when $W_I/d \gg 1$.

We will now compare the flux and flux divergence values as obtained with the detailed and simplified line transport models. The interplay between the spatial temperature gradient and the absorption parameters of the lines is particularly important in the flux divergence calculation. Hence it was essential that a realistic temperature distribution be used in the comparison. The temperature profile selected was that obtained from a coupled shock layer stagnation solution and is shown in Fig. 6 for the noted flight conditions. In order to make the comparison consistent, the detailed line-by-line calculation considered only those lines that were averaged in the equivalent line model (i.e., those lines at frequencies less than about 12.0 eV). There exist additional lines above 12.0 eV but these are strongly attenuated by the continuum absorption processes and hence contribute little to the total flux and flux divergence values.

A comparison of the net flux at three shock layer locations is shown in Table II.

TABLE II. Comparison of the Net Flux Obtained Using the Two Transport Models

Physical Location y/δ	Lines Only Flux, W/cm^2		Lines & Continuum Flux, W/cm^2	
	Detailed line-by-line	Five equivalent line	Detailed line-by-line	Five equivalent line
0 (wall)	4.00×10^3	3.73×10^3	9.05×10^3	8.78×10^3
.440	2.57×10^3	2.45×10^3	6.09×10^3	5.97×10^3
1.0 (shock)	8.55×10^3	8.70×10^3	1.87×10^4	1.89×10^4

As Table II indicates, the simplified model accurately approximates the line flux with a maximum error of about 8% at the wall. When the continuum flux is added (the same continuum flux values are used with the two line transport models) the error in using the approximate line transport model becomes less than 5%.

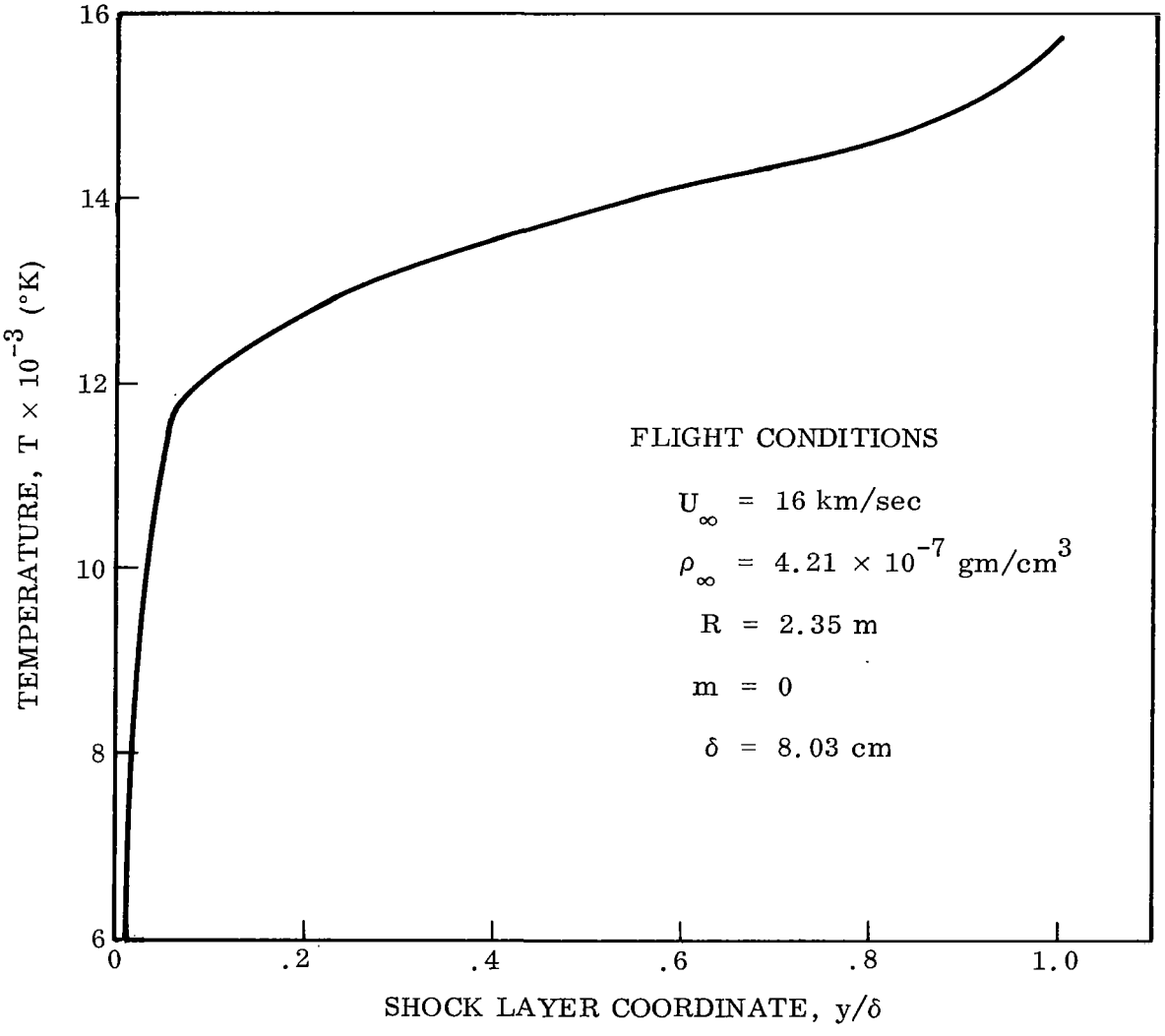

Fig. 6 Temperature Distribution Used In Comparing the Detailed and Simplified Line Transport Models

A comparison of the total (continuum plus lines) flux divergence values obtained from the two models is shown in Fig. 7. The common continuum contribution is shown so that the role of the line transport may be assessed. The agreement is surprisingly close with a maximum difference of about 10% at $y/\delta = .13$ and generally much less than 10%. Based on this comparison which, although for a single shock layer calculation, evaluates the two models over a wide range of temperatures, the simplified five-line model was felt to provide an adequate treatment for calculating the total transport.

As mentioned previously, the discussion of the equivalent line model has considered only nitrogen lines. In solving coupled flow problems with mass injection, it was necessary to include carbon and oxygen lines. The detailed set of relations derived for the equivalent line parameters of an arbitrary mixture of C, N, and O atoms are given in Appendix B.

An important transport effect was noticed early in our study of line radiation. This effect is common to both the detailed and simplified models. Namely, the temperature discontinuity at the shock front allows a fluid particle at the shock front to lose energy in strong resonance lines of the neutral and ionized atoms at a very large rate. However, as the fluid particle flows away from the shock, the energy radiated in these resonance lines rapidly becomes trapped resulting in a very large gradient in the flux divergence at the shock front. Calculations were made which showed that although the energy loss rates were very large initially, the times over which a particle loses energy at this rate are very small for typical superorbital entry conditions. Hence, the net effect of the initially large flux divergence values is to produce a negligible amount of radiative cooling. In order to avoid the numerical problems of handling the large flux divergence gradients at the shock, our coupled flow calculations begin the numerical integration of the flux divergence term at $\eta < 1.00$. However, even at $\eta = .98$ the flux divergence typically has dropped an order of magnitude and is relatively slowly varying. Finally, we should emphasize that this treatment of the flux divergence right behind the shock appears justified for $U_\infty \lesssim 50{,}000$ ft/sec. However, at substantially higher velocities, it may be necessary to reexamine this problem.

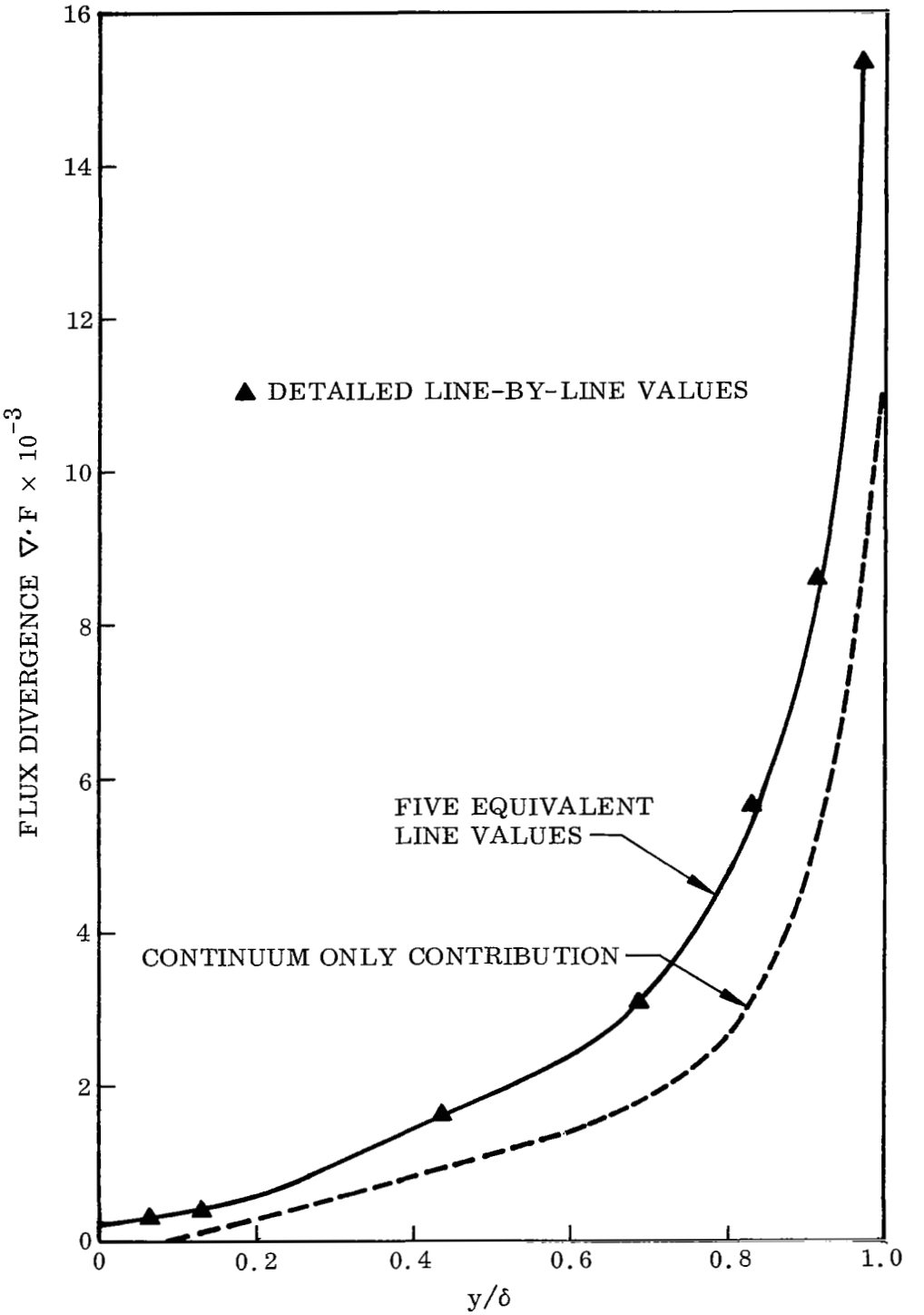

Fig. 7 Flux Divergence Values Obtained Using the Simplified and Detailed Line Transport Models

Section 5
RESULTS OF COUPLED FLOW CALCULATIONS

5.1 COMPARISON OF VISCOUS AND INVISCID SOLUTIONS

It is of interest to assess the role of viscous effects in structuring the shock layer under conditions of large surface mass injection and coupled radiative transport. Since time did not permit the extension of the inviscid analysis to include radiative transport in atomic lines, the viscous solutions used for comparison with the inviscid cases were correspondingly limited to continuum only transport. In Fig. 8, a comparison is given of the tangential velocity field along the stagnation line of a spherical body (R = 2.75 m) moving at a velocity U_∞ = 15.25 km/sec through an ambient density of ρ_∞ = 2.06×10^{-7} gm/cm^3.

As a result of radiative heating of ablation products, the density across the ablation layer-air interface is nearly continuous. Hence examination of the x-momentum equation shows that the tangential velocity should also be nearly continuous. Our solution shows a large discontinuity in tangential velocity at the interface due to the approximate integral solution employed. On the other hand, it was shown in Section 2 that the velocity distribution in the viscous layer solution as obtained using a quadratic profile is also in error (cf. Fig. 2). Unfortunately these errors in the velocity field distort the comparison of the viscous and inviscid solutions. Nonetheless it is of interest to compare the shock layer temperature and ablation product distributions from these two solutions. This is done in Fig. 9 where we note that the inviscid solution yields a significantly larger region occupied by the ablation product gases. The role of viscosity is also evident in comparing the temperature distributions shown in Fig. 9. For the viscous solution, the temperature begins to increase immediately due to conduction and then rises rapidly as the opacity of the ablation products increases. For the

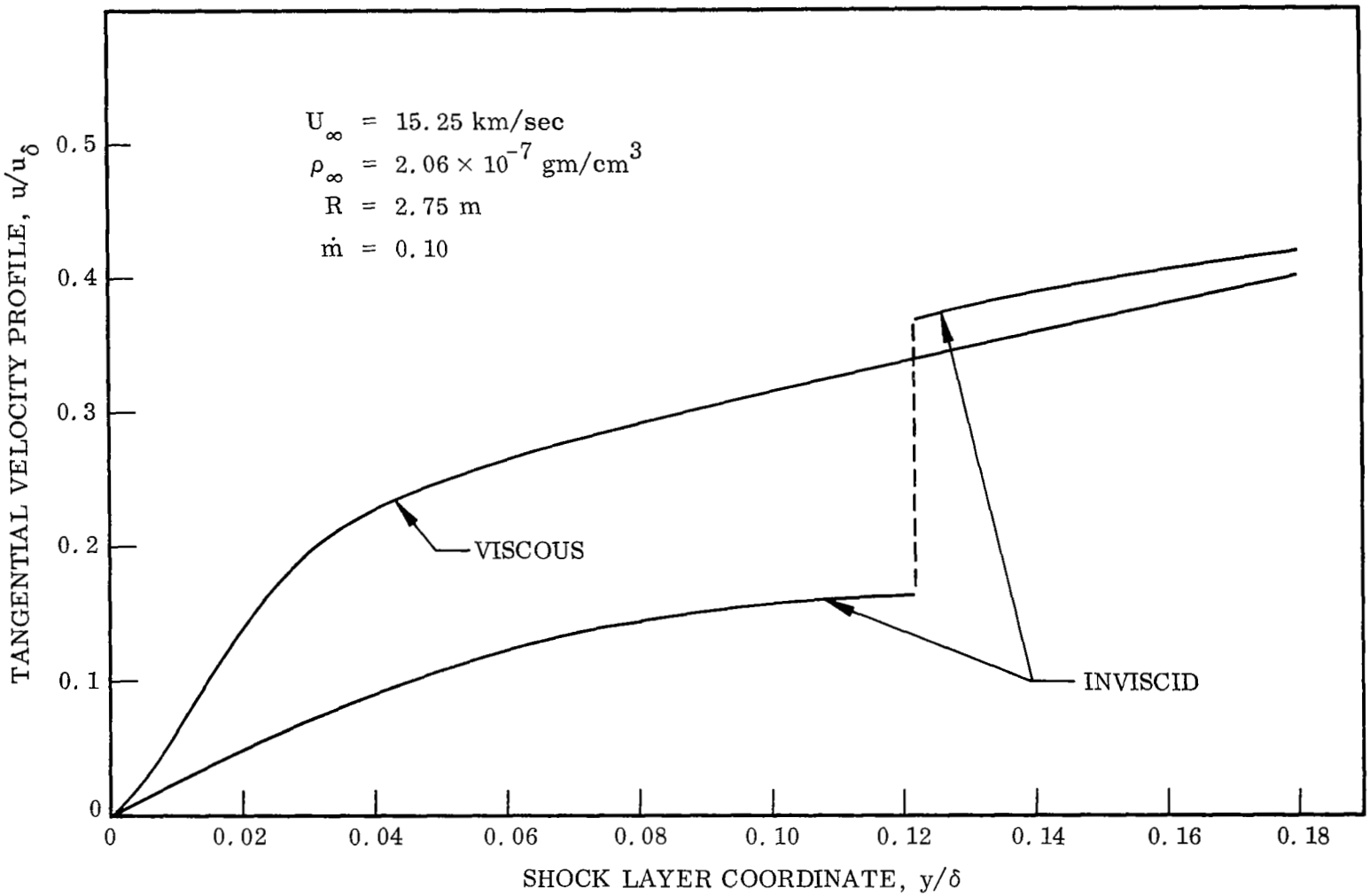

Fig. 8 Comparison of the Velocity Profiles Calculated Using an Inviscid and Viscous Analysis

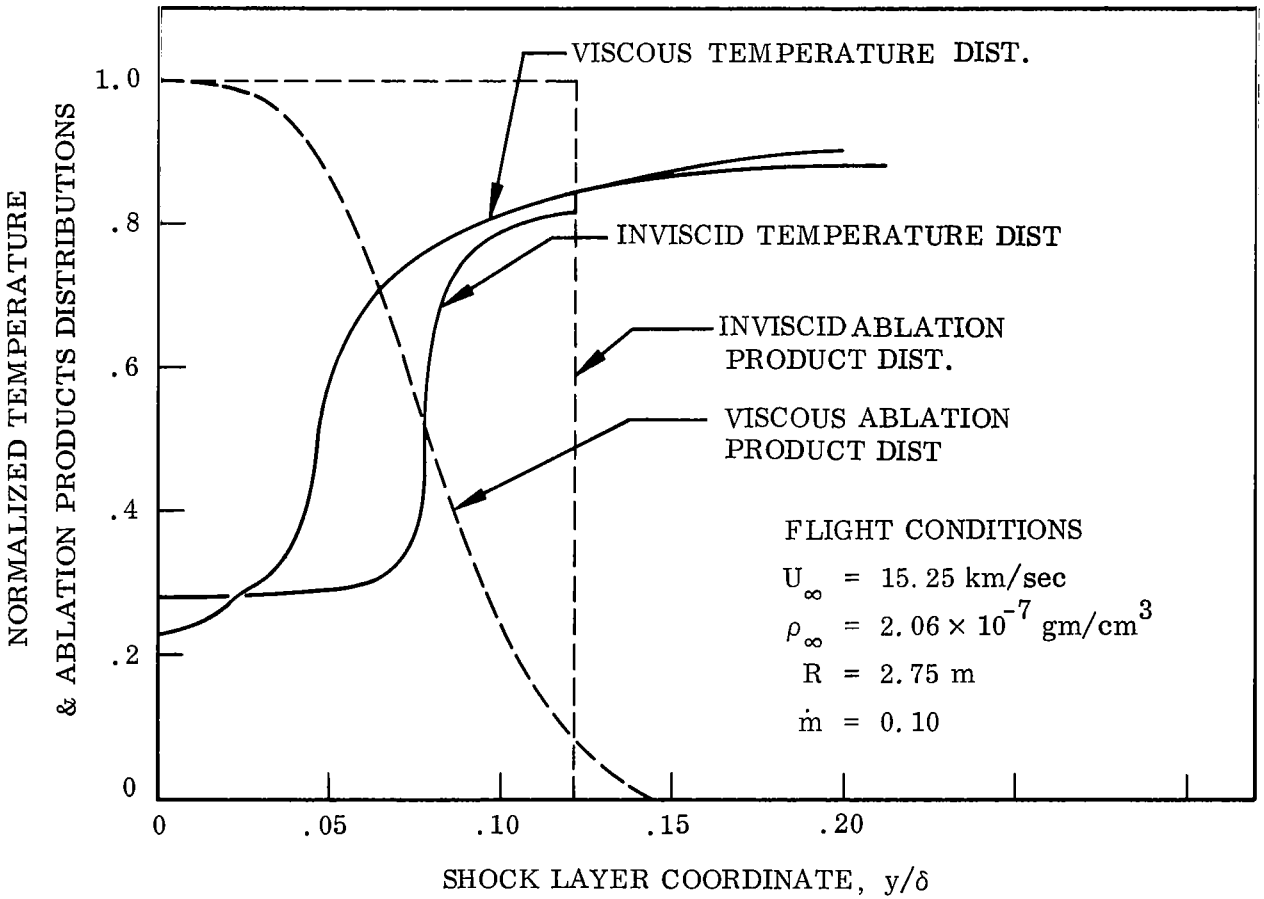

Fig. 9 Comparison of Shock Layer Properties Using a Viscous or Inviscid Analysis

inviscid solution, the ablation products are nearly transparent at the wall temperature and hence the temperature is almost constant near the wall. However, once the ablation product gas is heating to the point where its opacity is large, heating occurs rapidly and the ablation gases reach a temperature nearly equal to that at the edge of the air layer. The fact that the air and ablation product gases are quite opaque over much of the high frequency portion of the spectrum (roughly $h\nu > 10$ eV) and that for an inviscid model a condition of radiative equilibrium ($\cdot F' = 0$) is reached at the interface where $\rho v = 0$, forces this near continuity of temperature. Thus, although the effects of conduction can be seen near the wall, conduction plays a minor role in the overall heating of the ablation gases.

As a result of the differences in shock layer structure, primarily the difference in species distribution, the viscous and inviscid analyses yield a difference in the radiative flux reduction due to mass injection. This flux reduction is shown in Fig. 10, as a function of the normalized surface mass injection rate for the indicated flight conditions. Due to numerical difficulties it was not possible to extend the viscous solutions beyond $\dot{m} = 0.10$. On the other hand, the inviscid solution is invalid for mass flux rates below $\dot{m} = 0.10$. At the single point of common comparison, the viscous solution predicts a reduction to about 0.60 while the inviscid solution predicts a reduction of about 0.47; a relative difference of about 25%.

5.2 EFFECTS OF LINE TRANSPORT

While the importance of line transitions in radiative transport in uniform gases is now well recognized, only recently have line transitions been accounted for in coupled radiative-gasdynamic calculations. To the author's knowledge the only published work in which lines are treated is that of Dirling et al. (Ref. 19) and Page et al. (Ref. 20). We have compared our solution with those of Dirling et al. in Fig. 11. The two solutions differ considerably right behind the shock wave where Dirling shows a large temperature gradient. We believe this difference is due in part to the grey gas flux divergence model. Also, Dirling's value for the surface radiative flux is a factor of four less than ours. This difference is due presumably to the

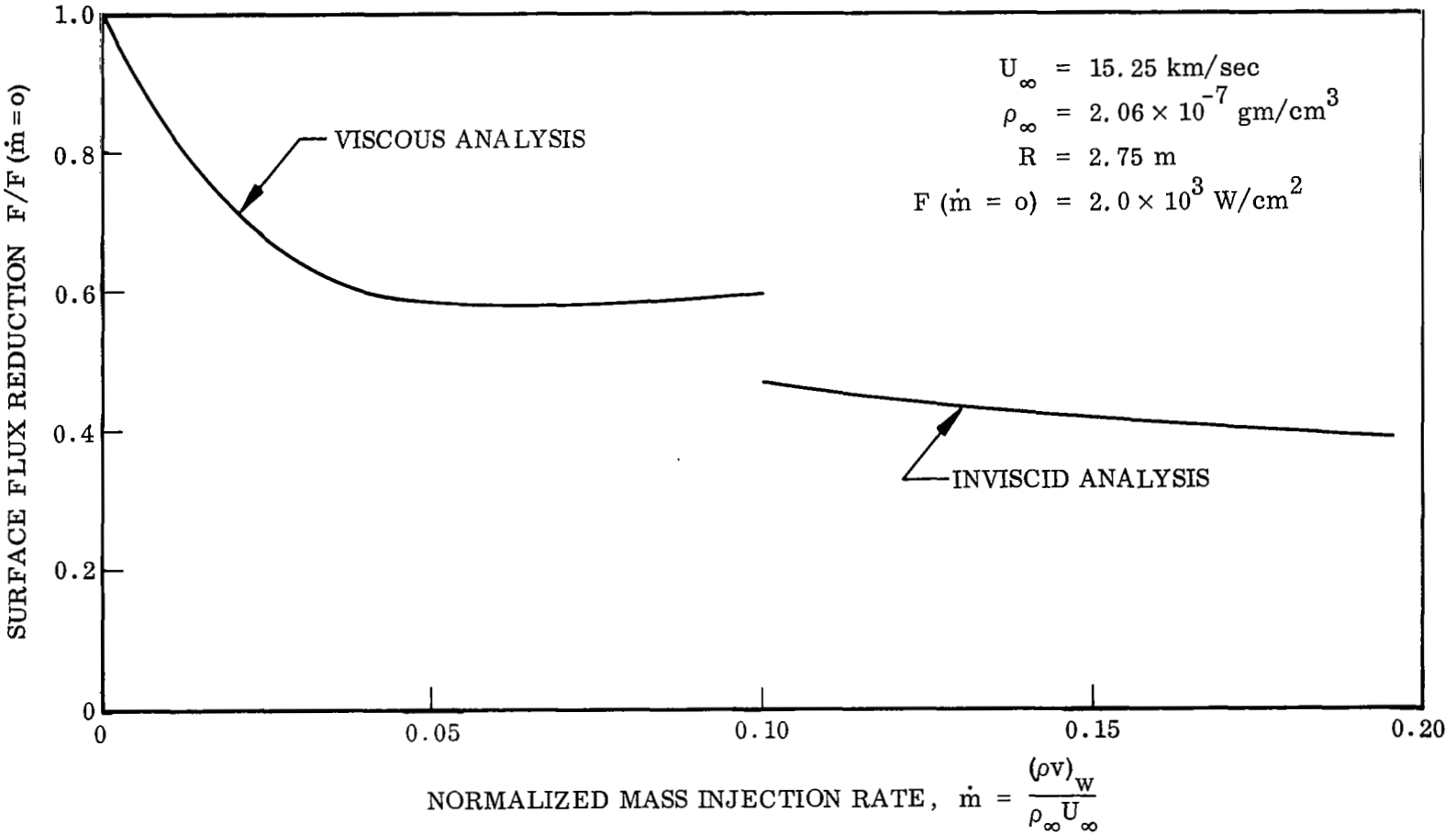

Fig. 10 Radiative Flux Reduction Due to Mass Injection (Continuum Only)

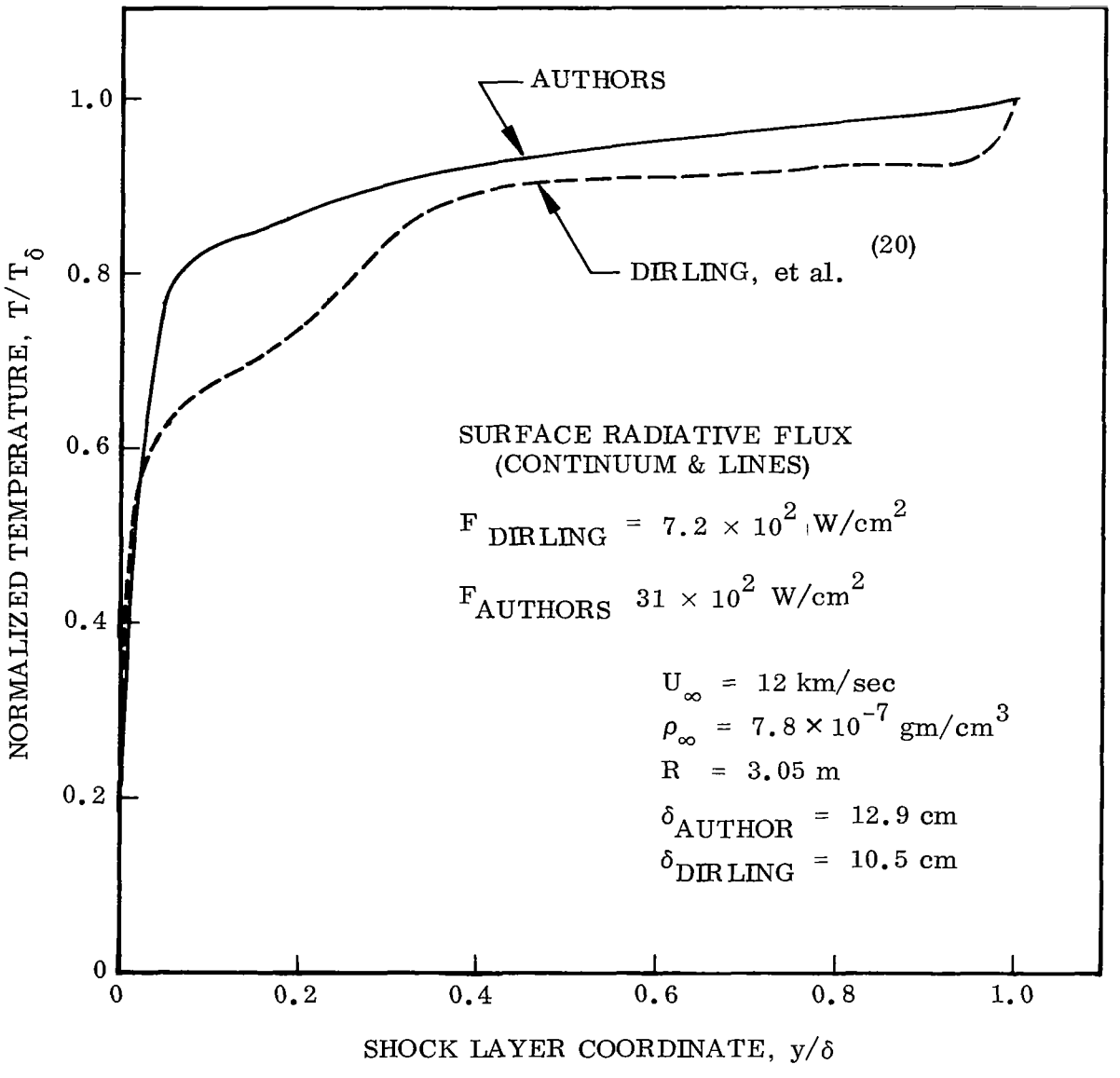

Fig. 11 Comparison of Shock Layer Temperature Distributions of Dirling and Authors

lower shock layer temperatures and resultant reduced emission in Dirling's solution. A comparison with the recent results of Page et al. (Ref. 20) is shown in Fig. 12. While Page and the authors have used essentially the same atomic cross sections for both continuous and discrete processes, the transport models are different. Despite the difference, the agreement in the enthalpy levels is quite close in the inviscid region of the shock layer. (Since Page's calculation is based on an inviscid flow analysis, the comparison is valid only in the inviscid region.) The values for spectrally integrated radiative flux are also in good agreement, although detailed spectral comparisons show major differences.

The relative effects of lines in comparison with a continuum-only calculation on the shock layer enthalpy is shown in Fig. 13 for the conditions noted. The increased emission from lines reduces the enthalpy below the continuum-only solution by a maximum of about 10%. This additional cooling significantly reduces the net increase in the surface radiative flux when line emission and absorption processes are included in coupled shock layer solutions. Table III summarizes the relative effect of including lines at velocities of 13.7, 15.25, and 16.8 km/sec.

TABLE III Effect of Lines on Surface Radiative Flux
($\rho_\infty = 2.06 \times 10^{-7}$ gm/cm^3; R = 2.75 m; $\dot{m} = 0$)

Velocity (km/sec)	Radiative Flux, W/cm^2 (Continuum only)	Radiative Flux, W/cm^2 (Continuum plus lines)
13.7	1.15×10^3	1.67×10^3
15.25	2.02×10^3	3.22×10^3
16.8	3.48×10^3	4.70×10^3

We see from these results that the net increase in radiative flux due to lines is about 50%.

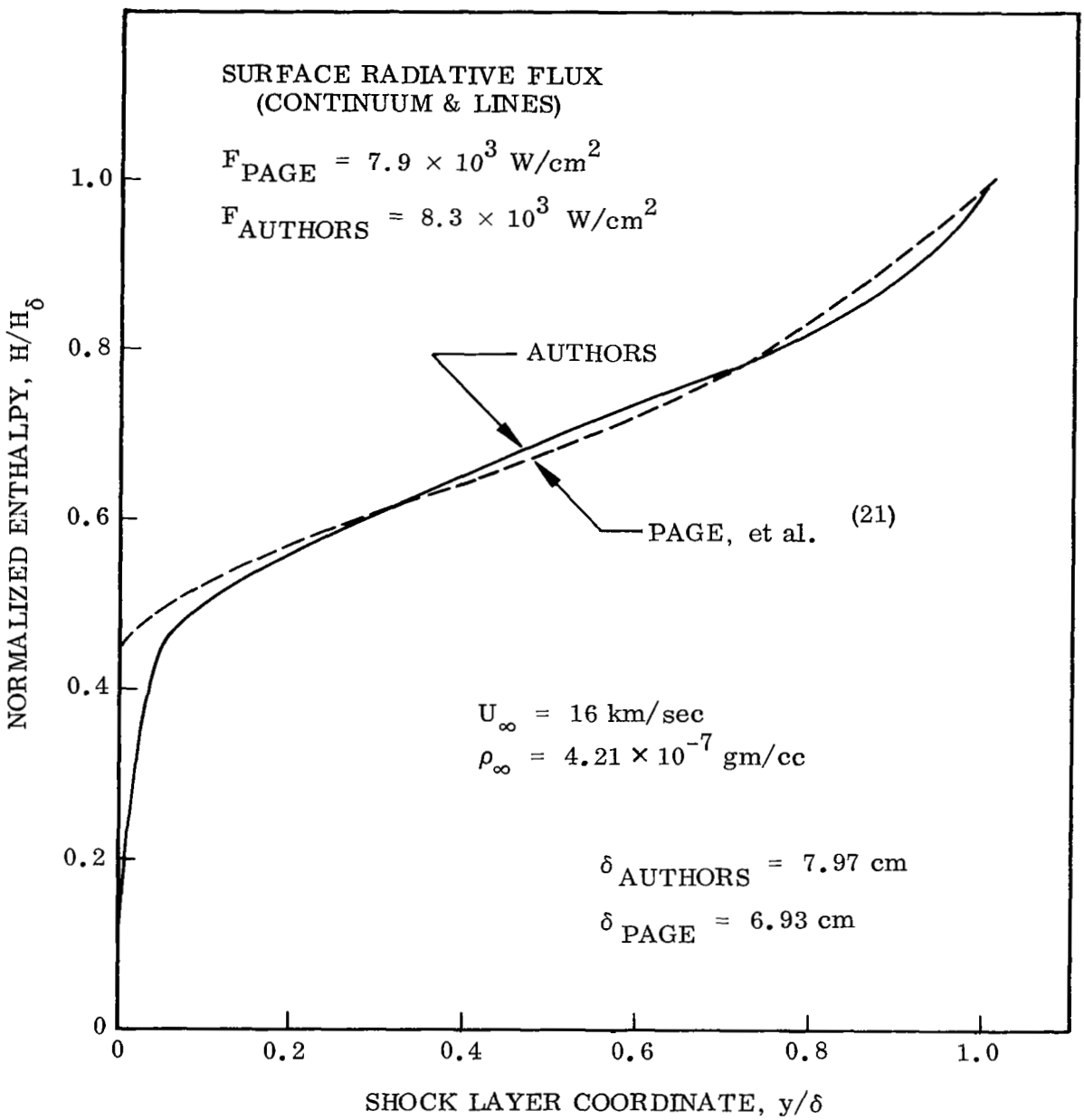

Fig. 12 Comparison of Shock Layer Enthalpy Distributions of Page and Author

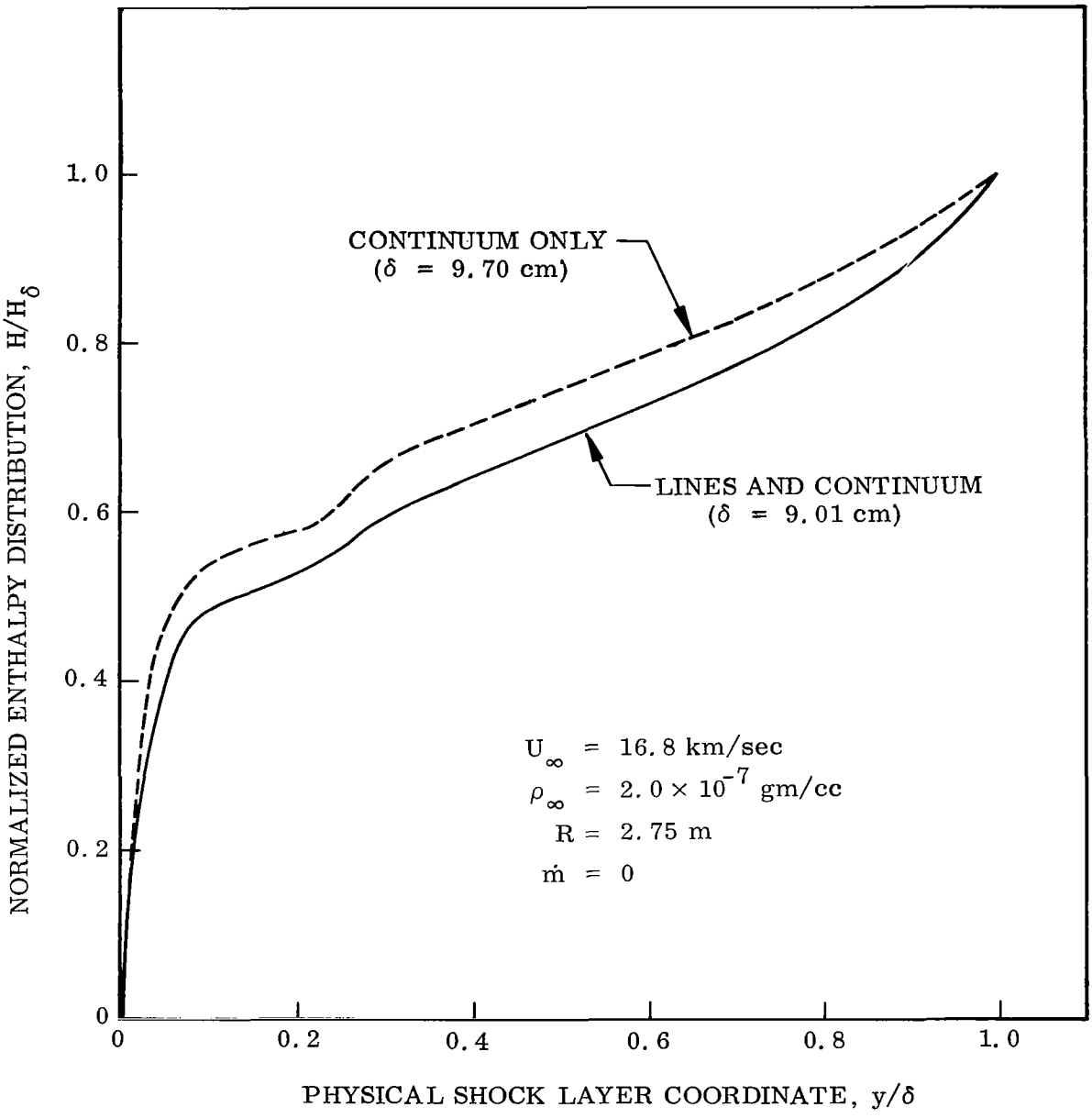

Fig. 13 Effect of Atomic Line Transport on Shock Layer Enthalpy Distribution

5.3 ABLATION PRODUCT ABSORPTION*

The various species contained in the ablation product gases have been shown previously in Fig. 10 to absorb strongly the radiative flux emitted in the high temperature regions of the shock layer. It is of interest to determine what species are primarily responsible for this absorption. In Fig. 14 we present, for the case of a continuum-only solution, the monochromatic radiative flux incident at the surface with and without mass injection of ablation products as calculated using a viscous analysis. It is clear from this spectral plot that most of the absorption is due to neutral carbon atoms which block the energy emitted towards the wall at frequencies greater than 11.2 eV ground state photoionization limit. Some absorption by molecular bands is apparent but this occurs at frequencies where the monochromatic radiative flux emitted in the high temperature regions towards the wall is quite low. The net effect of including or omitting the absorption due to molecular species is given in Fig. 15. We see that molecular absorption accounts for a relatively small but nonnegligible portion of the flux reduction.

Solutions were obtained including the combined effects of radiative transport in atomic lines and mass injection. The line transport used a six group model with f-numbers and half-widths of each group averaged between carbon, nitrogen, and oxygen atoms. (Hydrogen lines were neglected.) The line-grouping transport model implies that all lines within a given group emit and absorb at a common frequency. While this type of model is valid for a system with a fixed ratio of elemental C, N, and O throughout the radiating layer, it breaks down, in general, for a layer containing mainly C atoms in one region and N and O atoms in another.** For such a nonuniform distribution of species, the line grouping model is valid only if there is strong overlapping between the carbon, nitrogen, and oxygen transitions. However, an a posterori check of the equivalent widths

---

*All solutions discussed in this section are based on a viscous analysis. The ablation gases are the pyrolysis products of carbon phenolic ($C_{\tilde{C}}$ = .929; $C_{\tilde{H}}$ = .019; $C_{\tilde{O}}$ = .051).

**The authors are indebted to Mr. Dale Compton, NASA Ames Research Center, for bringing this point to their attention.

of the lines within the various line groups showed these lines to be, for the most part, well isolated. Because of this result, the calculated amount of absorption of line radiation by the ablation product gases was significantly overpredicted. Hence the results of the combined solutions with line transport and mass injection were not valid and are not presented here. Further work on a valid line transport model for multi-specie atomic gases is required.

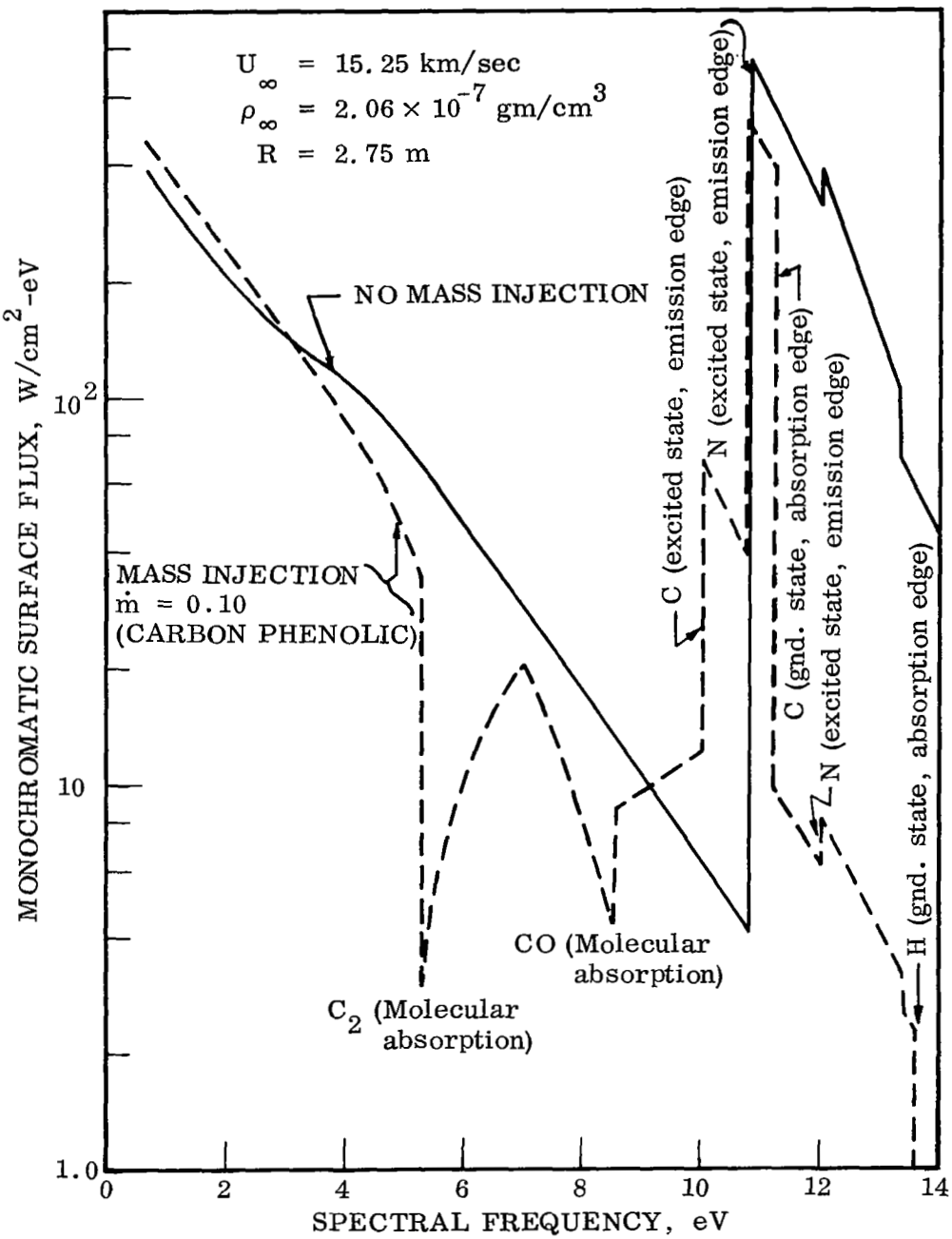

Fig. 14 Spectral Attenuation of the Radiative Flux by Ablation Products, Viscous Analysis (Continuum Only)

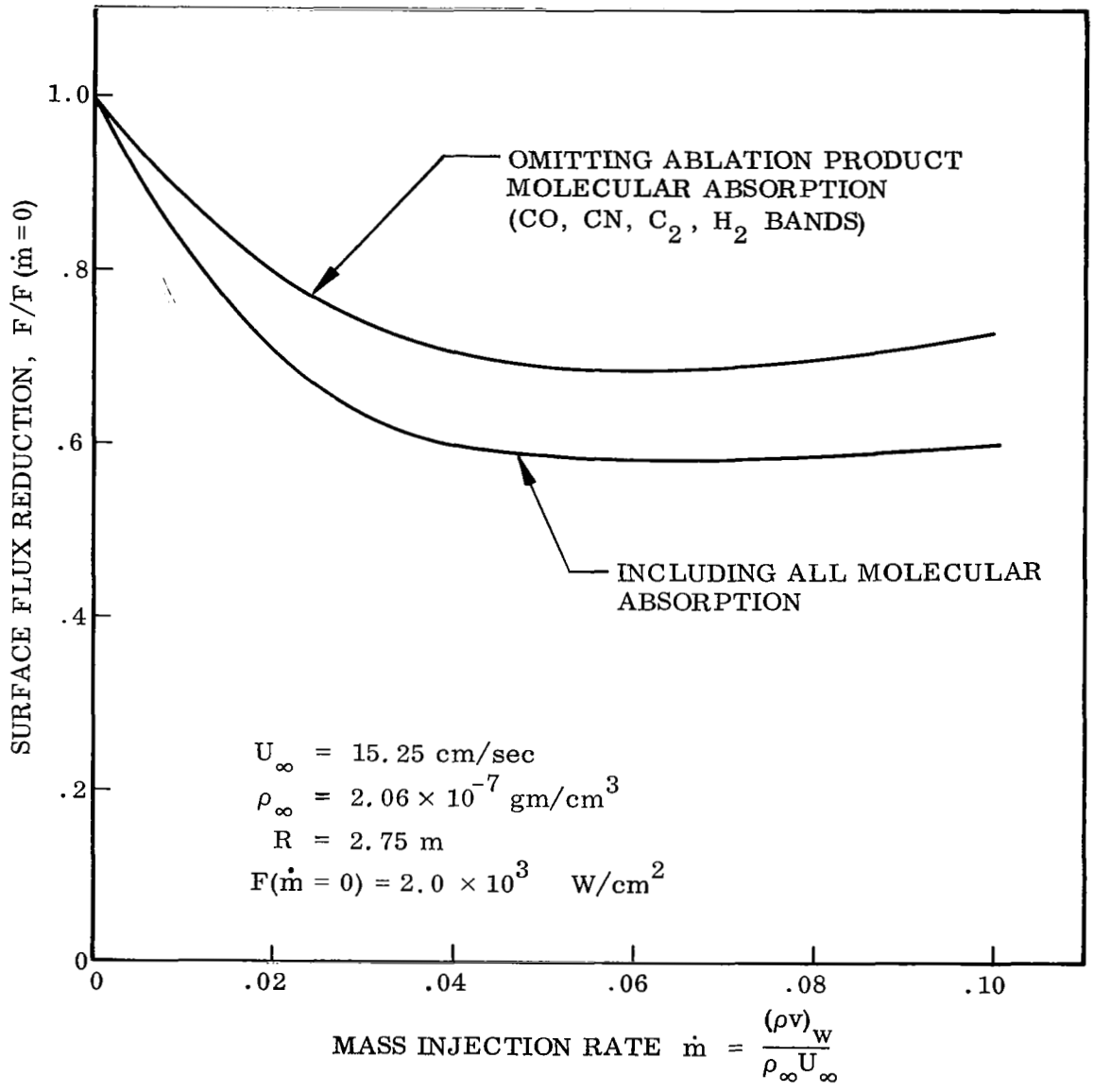

Fig. 15 Effect of Molecular Species on Ablation Product Flux Reduction (Continuum Only)

Section 6
CONCLUSIONS

The effects of ablation product absorption and atomic line transitions on radiative transport within the shock layer enveloping an ablating blunt body have been examined. This work has extended our previous studies (Refs. 3, 4) to higher mass injection rates. Contrary to our earlier conclusions,* we now find that the radiative flux from the high temperature portion of the shock layer is significantly reduced by surface mass injection of ablation product gases with rates of the order of a few percent of the free stream mass flux. The flux reduction is due mainly to absorption by atomic carbon and hydrogen; molecular species provide only a modest addition to the flux reduction.

Both a viscous and an inviscid analysis were employed. The viscous analysis suffers from numerical difficulties as the mass injection rate parameter f_w approaches roughly a valud of 10. The inviscid analysis is applicable at very high blowing rates being limited only by the thin shock layer approximation. However, the inviscid analysis becomes invalid as the blowing parameter becomes small, roughly a value of 10. Hence there is only a small region of overlap in applicability of the viscous and inviscid solutions. Both the viscous and inviscid analysis show the same qualitative behavior of a weak dependence of surface radiative flux reduction on mass injection rate (that is once the injection level is relatively high, $f_w \gtrsim 1$). A quantitative comparison of the inviscid and viscous analysis at the single common mass injection condition showed that the solutions agreed in predicting the surface flux reduction to within about 25%. Further quantitative comparison requires improvement in the flow field solution in both the viscous and inviscid analyses. More exact inviscid treatments have recently become available (Ref. 22). It is

*The conclusions deduced in Ref. 4 to which we are referring were, in part, affected by erroneous numerical computations of the species conservation equations.

recommended that the flow field solution in the viscous analysis be obtained by exact numerical integration of the momentum equations. This extension would permit a quantitatively meaningful assessment of the effects of molecular transport processes on shock layer radiative transfer.

The role of atomic line transitions in viscous, radiating shock layers were examined. Atomic lines increase the level of radiant energy transport within the shock layer by about a factor of two and hence were expected to increase the surface radiative flux. However, the increased energy loss through the shock front moderates the effects of line transport yielding a net increase over a continuum-only calculation of the surface radiative flux of about 50% at velocities between 12-16 km/sec. The coupled radiating flow solution used a simplified line transport model. The validity of this model was based on a comparison with a more detailed line-by-line calculation. However, the validity of the model was established for a system of nitrogen lines only. Further work on the line transport problem is needed to develop a simplified model valid for mixtures of H, C, N and O atoms and ions over a wide range of thermodynamic conditions.

Section 7
REFERENCES

1. Wilson, K. H., and Hoshizaki, H., "Inviscid, Nonadiabatic Flow About Blunt Bodies," AIAA Journ., 3, No. 1, 67-74 (Jan. 1965).

2. Hoshizaki, H., and Wilson, K. H., "The Viscous, Radiating Shock Layer About a Blunt Body," AIAA Journ. 3, No. 9, 1614-1622 (Sept. 1965).

3. Hoshizaki, H., and Wilson, K. H., "Convective and Radiative Heat Transfer During Superorbital Entry," AIAA Journ., 5, No. 1, 25-35 (Jan. 1967).

4. Hoshizaki, H., and Lasher, L. E., "Convective and Radiative Heat Transfer to an Ablating Body," LMSC 4-06-66-12, July 1966.

5. Hayes, W. D., and Probstein, R. F., Hypersonic Flow Theory, Academic Press, New York (1959), pp. 388-389.

6. Smith, A. M. O., and Clutter, D. W., "Solution of the Incompressible, Laminar Boundary-Layer Equations," AIAA Journ. 1, No. 9, 2062-2071 (1963).

7. Maslen, S. H., and Moeckel, W. E., "Inviscid Hypersonic Flow Past Blunt Bodies," J. Aerospace Sci. 24, No. 9, 683-693 (1957).

8. Zeiberg, S. L., "Similar Laminar Boundary Layer With Large Injection," AIAA Journ. 4, No. 1, 157-158 (Jan. 1966).

9. DeRienzo, P., and Pallone, A., "Convective Stagnation Point Heating for Reentry Speeds up to 70,000 Feet/Second Including Effects of Large Blowing Rates," AVCO R&D Div., RAD-TM-65-58, Jan. 1966.

10. Lees, L., "Convective Heat Transfer With Mass Addition and Chemical Reactions," Combustion and Propulsion, Third AGARD Colloquium (March 17-28, 1958), Palermo, Sicily.

11. Viegas, L. R., and Howe, J. T., "Thermodynamic and Transport Property Correlation Formulas for Equilibrium Air From 1000°K to 15,000°K," NASA TN D-1429, Oct. 1962.

12. Howe, J. T., and Sheaffer, Y. S., "Effects of Uncertainties in the Thermal Conductivity of Air on Convective Heat Transfer for Stagnation Temperature up to 30,000°K," NASA TN D-2678, Feb. 1965.

13. Thomas, P. D., and Wilson, K. H., "Fireball Ablation: Vol. I, Quasi-Steady Analysis of Ablation in Supersonic and Hypersonic Flow," USAF, AFFDL-TR-66-87, Vol. I (Secret), April 1966.

14. Biberman, L. M., et al., "Radiation Heating in Hypersonic Flow," Cosmic Research 2, 376-387 (1964).

15. Allen, R. A., "Radiation Graphs, Spectrally Integrated Fluxes Including Line Contributions and Self-Absorption," AVCO-Everett Research Lab., RR-230, Sept. 1965.

16. Zel'dovich, Ya. B., and Raizer, Yu. P., Physics of Shock Waves and High-Temperature Hydrodynamic Phenomena, Chapter II, Academic Press, New York (1966).

17. Wilson, K. H., and Greif, R., "Radiation Transport in Atomic Plasmas," LMSC 6-77-67-31, Nov. 1967.

18. Wilson, K. H., and Nicolet, W. E., "Spectral Absorption Coefficients of Carbon, Nitrogen and Oxygen Atoms," LMSC 4-17-66-5, Nov. 1966.

19. Plass, G. N., "Models for Spectral Band Absorption," JOSA 48, 690-703 (1958).

20. Dirling, R. B., Jr., Rigdon, W. S., and Thomas, M., "Stagnation-Point Heating Including Spectral Radiative Transfer," Proceedings of 1967 Heat Transfer and Fluid Mechanics Institute, June 1967.

21. Page, W. A., Compton, D. L., Borucki, W. J., Ciffone, D. L., and Cooper, D. M., "Radiation Transport in Inviscid, Nonadiabatic Stagnation-Region Shock Layers," to be presented to AIAA 3rd Thermophysics Conference, June 24-26, 1968.

22. Chin, J. H., "Radiation Transport for Stagnation Flows Including the Effects of Lines and Ablation Layer," to be presented at AIAA Fluid and Plasma Dynamics Meeting, June 24-26, 1968, Los Angeles, Calif.

23. Biberman, L. M., and Norman, G. E., "Recombination Radiation and Bremsstrahlung of a Plasma,"

APPENDIX A

CONTINUUM ABSORPTION COEFFICIENT FOR ATOMIC AND MOLECULAR SPECIES

The continuum absorption coefficients for the neutral and ionized atoms of H, C, N, and O were calculated using the approximate relations derived by Biberman and Norman (Ref. 23) for photoionization from excited states and the tabulation of Wilson and Nicolet (Ref. 18) for photoionization from low-lying states. The absorption due to free-free transitions was included using the hydrogenic approximation. The equations given here hold over the frequency range $0 < h\nu < 20$ eV.

The following variables and constants are defined (the subscript k denotes the various species H, H^+, C, C^+, N, N^+, O, O^+):

$\tilde{a}$ = constant = 7.25×10^{-16} cm^2 eV^2

$(\epsilon_I)_k$ = ionization energy (Table A.1), eV

$(\epsilon_T)_k$ = threshold energy (Table A.1), eV

Γ_k = statistical weight factor* (Table A.1)

ξ_k = nonhydrogenic correction factor (Fig. A.1)

θ = temperature kT in energy units, eV

u = frequency $h\nu$ in energy units, eV

N_k = number density of specie k, part/cm^3

Σ_k = partition function for specie k

*We note that Biberman and Norman (Ref. 23) define Γ_k as a ratio of the temperature dependent partition functions of parent atom and residual ion. However, we have found that selecting Γ_k = constant = $2g_{II}/g_I$ (where g_{II} is the ground state statistical weight of the residue ion and g_I the ground state statistical weight of the parent atom) gives a better fit to the detailed data of Ref. 18.

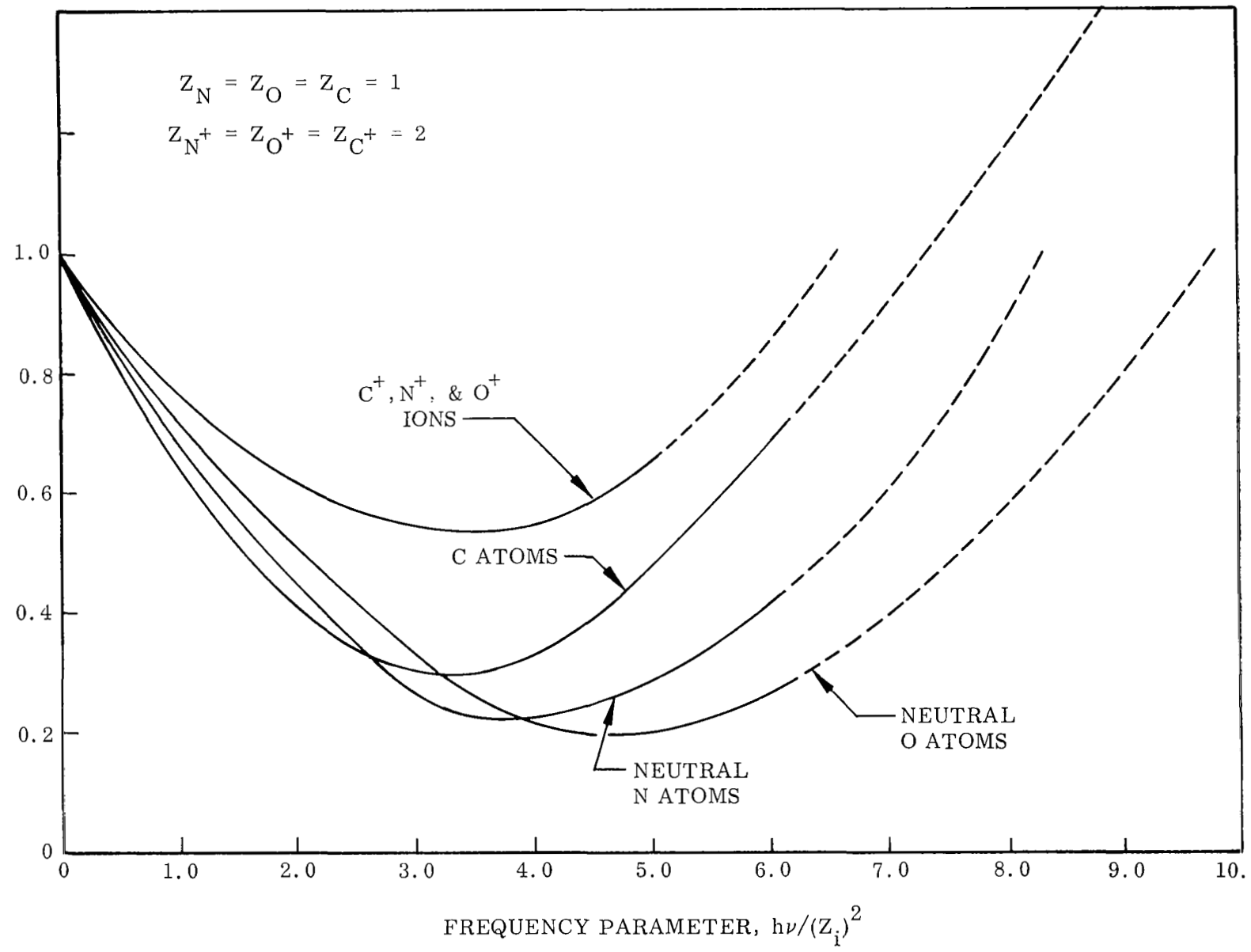

Fig. A-1 Quantum-Mechanical Correction Factor $\xi(h\nu)$

TABLE A.1

ATOMIC CONSTANTS FOR CONTINUUM ABSORPTION COEFFICIENTS

Species k	$(\epsilon_I)_k$ eV	$(\epsilon_T)_k$ eV	Γ_k
H	13.6	0.80	1
H^+	-	-	-
C	11.26	3.78	1.33
C^+	24.4	14.9	.333
N	14.54	4.22	4.50
N^+	29.6	18.1	1.33
O	13.61	4.25	0.888
O^+	35.1	20.4	4.50

EQUATIONS FOR H

for $0 < u < 0.80$ eV

$$(\mu_H)_1 = N_H \tilde{a}\, \theta\Gamma e^{-(\epsilon_I - u)/\theta} \xi(u)/u^3$$

for $0.80 \text{ eV} \leq u < 1.60$ eV

$$(\mu_H)_2 = (\mu_H)_1 \, e^{-(u-\epsilon_T)/\theta}$$

for $1.60 \text{ eV} \leq u < 3.40$ eV

$$(\mu_H)_3 = (\mu_H)_2 + 2.6 \times 10^{-16} N_H \left(\frac{1.6}{u}\right)^3 e^{-(\epsilon_I - 1.60)/\theta}$$

for $3.40 \text{ eV} \leq u < 13.6 \text{ eV}$

$$(\mu_H)_4 = (\mu_H)_3 + 1.12 \times 10^{-16} N_H \left(\frac{3.40}{u}\right)^3 e^{-(\epsilon_I - 3.40)/\theta}$$

for $13.6 \text{ eV} \leq u$

$$(\mu_H)_5 = (\mu_H)_4 + 5.92 \times 10^{-18} N_H \left(\frac{13.6}{u}\right)^3$$

EQUATIONS FOR H^+ (FREE-FREE)

Not included.

EQUATIONS FOR C

for $0 < u < 3.78 \text{ eV}$

$$(\mu_C)_1 = N_C \tilde{a} \theta \Gamma e^{-(\epsilon_I - u)/\theta} \xi(u)/u^3$$

for $3.78 \text{ eV} \leq u < 6.83 \text{ eV}$

$$(\mu_C)_2 = (\mu_C)_1 e^{-(u - \epsilon_T)/\theta}$$

for $6.83 \text{ eV} \leq u < 8.33 \text{ eV}$

$$(\mu_C)_3 = (\mu_C)_2 + 5 \times 10^{-17} \frac{N_C}{\Sigma_C} e^{-4.18/\theta}$$

for $8.33 \text{ eV} \leq u < 9.75 \text{ eV}$

$$(\mu_C)_4 = (\mu_C)_3 + 2.2 \times 10^{-17} \frac{N_C}{\Sigma_C} e^{-2.68/\theta}$$

for $9.75 \text{ eV} \leq u < 11.0 \text{ eV}$

$$(\mu_C)_5 = (\mu_C)_4 + 8.5 \times 10^{-17} \frac{N_C}{\Sigma_C} e^{-1.26/\theta}$$

for $u > 11.0 \text{ eV}$

$$(\mu_C)_6 = (\mu_C)_5 + 9.9 \times 10^{-17} \frac{N_C}{\Sigma_C}$$

EQUATIONS FOR C^+

for $0 < u < 15.1 \text{ eV}$

$$(\mu_{C^+})_1 = N_{C^+} \, 4 \, \tilde{a} \, \theta \, \Gamma \, e^{-(\epsilon_I - u)/\theta} \, \xi(u)/u^3$$

for $15.1 \text{ eV} \leq u < 18.8 \text{ eV}$

$$(\mu_{C^+})_2 = (\mu_{C^+})_1 \, e^{-(u-\epsilon_T)/\theta}$$

for $u > 18.8 \text{ eV}$

$$(\mu_{C^+})_3 = (\mu_{C^+})_2 + 6.8 \times 10^{-17} \left(\frac{N_{C^+}}{\Sigma_{C^+}}\right) e^{-5.33/\theta}$$

EQUATIONS FOR N

for $0 < u < 4.22$ eV

$$(\mu_N)_1 = N_N \tilde{a} \theta \Gamma e^{-(\epsilon_T - u)/\theta} \xi(u)/u^3$$

for $4.22 \text{ eV} \leq u < 10.8$ eV

$$(\mu_N)_2 = (\mu_N)_1 e^{(u-\epsilon_T)/\theta}$$

for $10.8 \text{ eV} \leq u < 11.9$ eV

$$(\mu_N)_3 = (\mu_N)_2 + 5.16 \times 10^{-17} \left(\frac{N_N}{\Sigma_N}\right) e^{-3.58/\theta}$$

for $11.9 \text{ eV} \leq u < 13.4$ eV

$$(\mu_N)_4 = (\mu_N)_3 + 6.4 \times 10^{-17} \left(\frac{N_N}{\Sigma_N}\right) e^{-2.38/\theta}$$

for $u \geq 14.3$ eV

$$(\mu_N)_5 = (\mu_N)_4 + 3.6 \times 10^{-17} \left(\frac{N_N}{\Sigma_N}\right)$$

EQUATIONS FOR N^+

for $0 < u < 11.5$ eV

$$(\mu_{N^+})_1 = N_{N^+} 4 \tilde{a} \theta \Gamma e^{-(\epsilon_I - u)/\theta} \xi(u)/u^3$$

for $u > 18.1$ eV

$$(\mu_{N^+})_2 = (N_{N^+})_1 \, e^{-(u-\epsilon_T)/\theta}$$

EQUATIONS FOR O

for $0 < u < 4.25$ eV

$$(\mu_O)_1 = N_O \, \tilde{a} \, \theta \, \Gamma \, e^{-(\epsilon_I - u)/\theta} \, \xi(u)/u^3$$

for $4.25 \text{ eV} \leq u < 13.36$ eV

$$(\mu_O)_2 = (\mu_O)_1 \, e^{-(u-\epsilon_T)/\theta}$$

for $u > 13.36$ eV

$$(\mu_O)_3 = (\mu_O)_2 + 3.6 \times 10^{-17} \left(\frac{N_O}{\Sigma_O}\right)$$

EQUATIONS FOR O^+

for $u > 0$

$$\mu_{O^+} = N_{O^+} \, 4 \, \tilde{a} \, \theta \, \Gamma \, e^{-(\epsilon_I - u)/\theta} \, \xi(u)/u^3$$

The absorption coefficient of various molecular band systems was included in terms of the usual pseudo-continuum smeared-line model. The selection of the band systems included was based on estimates of their significance in ablation layer absorption (Ref. 4). The particular band systems included, the maximum value of the absorption cross section, and the frequency interval spanned by the band are given in Table A.2. Further details on these molecular band absorption coefficients can be found in Ref. 4.

TABLE A.2

Molecule	Contribution	Cross-Section CM^2	Frequency Range For Significant Absorption, eV
H_2	Werner	3×10^{-17}	$11 \leq h\nu \leq 15.494$
	Photoionization	7×10^{-18}	$15.494 \leq h\nu \leq 25$
C_2	Swan	3×10^{-17}	$1.8 \leq h\nu \leq 6.0$
	Fox Herzberg	4×10^{-18}	$1.8 \leq h\nu \leq 5.35$
	Mulliken	3×10^{-17}	$5.35 \leq h\nu \leq 6.0$
	Freymark	6×10^{-18}	$1.8 \leq h\nu \leq 6.0$
CN	Violet	3×10^{-17}	$2.0 \leq h\nu \leq 6.0$
CO	4th Positive	2×10^{-18}	$7 \leq h\nu \leq 10$
N_2	Birge-Hopfield	1.2×10^{-17}	$11 \leq h\nu \leq 14.2$
O_2	Schuman-Runge	3.7×10^{-20}	$7 \leq h\nu \leq 9.2$

APPENDIX B

EQUIVALENT LINE PARAMETERS FOR AN ARBITRARY MIXTURE ON C, N, AND O ATOMS

The parameters $\bar{f}$, $\bar{\gamma}$, $\bar{\alpha}$ required for the line flux and flux divergence calculation are defined by Eq. (4), as derived in Section 4. Using the f-number and (half) half-width data from Reference 18, the coefficients in the defining equations were evaluated. The totality of lines considered have been grouped into six equivalent lines. For each equivalent line the algebraic expressions for $\bar{f}$, $\bar{\gamma}$, $\bar{\alpha}$ are listed below.

To account for the three different atomic species present within each group, the weight factors X_C, X_N, and X_O, defined by appropriate number density ratios, are introduced.

$$X_C = \frac{N_C}{N_T}$$

$$X_N = \frac{N_N}{N_T}$$

$$X_O = \frac{N_O}{N_T}$$

with $$N_T = N_C + N_N + N_O$$

In addition to the parameters $\bar{f}$, $\bar{\gamma}$, $\bar{\alpha}$ for each line we also state: the weighted number of lines n, the spectral interval D covered by the equivalent line, and the spectral location $h\nu$ of the equivalent line.

GROUP 1

$$\bar{f}_1 = \frac{1}{n_1} \{X_C f_C + X_N f_N + X_O f_O\}$$

$$f_C = \frac{1}{\Sigma_C} \{(12\ e^{-7.536/kT})\ 1.13 + (36\ e^{-8.646/kT})\ .835 + (60\ e^{-9.725/kT})\ .132\}$$

$$f_N = \frac{1}{\Sigma_N} \{(18\ e^{-10.452/kT})\ 1.07 + (54\ e^{-11.877/kT})\ .965 + (90\ e^{-13.002/kT})\ .156\}$$

$$f_O = \frac{1}{\Sigma_O} \{(8\ e^{-9.283/kT})\ 1.00 + (24\ e^{-10.830/kT})\ 1.04 + (40\ e^{-12.077/kT})^{1/2}\ .162^{-10}\}$$

$$\bar{\gamma}_1 = \frac{1}{n_{11}^2 f} \{X_C^{1/2}(\gamma_C f_C)^{1/2} + X_N^{1/2}(\gamma_N f_N)^{1/2} + X_O^{1/2}(\gamma_O f_O)^{1/2}\}^2$$

$$(\gamma_C f_C)^{1/2} = \left(\frac{1}{\Sigma_C}\right)^{1/2} \{(12\ e^{-7.536/kT})^{1/2}\ 8.14^{-11} + (36\ e^{-8.646/kT})^{1/2}\ 1.27^{-10} + (60\ e^{-9.725/kT})^{1/2}\ 3.17^{-10}\}$$

$$(\gamma_N f_N)^{1/2} = \left(\frac{1}{\Sigma_N}\right)^{1/2} \{(18\ e^{-10.452/kT})^{1/2}\ 7.10^{-11} + (54\ e^{-11.877/kT})^{1/2}\ 1.85^{-10} + (90\ e^{-13.002/kT})^{1/2}\ 1.85^{-10}\}$$

$$(\gamma_O f_O)^{1/2} = \left(\frac{1}{\Sigma_O}\right)^{1/2} \{(8\ e^{-9.283/kT})^{1/2}\ 3.89^{-11} + (24\ e^{-10.830/kT})^{1/2}\ 1.35^{-10} + (40\ e^{-12.077/kT})^{1/2}\ 9.94^{-11}\}$$

$$\bar{\alpha}_1 = n_1 \bar{f}_1^2 \frac{1}{\{X_C(f_C^2/\gamma_C) + X_N(f_N^2/\gamma_N) + X_O(f_O^2/\gamma_O)\}}$$

$$\frac{f_C^2}{\gamma_C} = \left(\frac{1}{\Sigma_C}\right) \{(12\ e^{-7.536/kT})\ 3.22^{20} + (36\ e^{-8.646/kT})\ 2.06^{19} + (60\ e^{-9.725/kT})\ 2.74^{16}\}$$

$$\frac{f_N^2}{\gamma_N} = \left(\frac{1}{\Sigma_N}\right) \{(18\ e^{-10.452/kT})\ 4.45^{20} + (54\ e^{-11.877/kT})\ 5.20^{19} + (90\ e^{-13.002/kT})\ 1.30^{17}\}$$

$$\frac{f_O^2}{\gamma_O} = \left(\frac{1}{\Sigma_O}\right) \{(8\ e^{-9.283/kT})\ 7.32^{20} + (24\ e^{-10.830/kT})\ 1.22^{20} + (40\ e^{-12.077/kT})\ 4.54^{17}\}$$

$$n_1 = 17\ X_C + 23\ X_N + 9\ X_O$$

$$D_1 = 1.175$$

$$(h\nu)_1 = 1.20$$

GROUP 2

$$\bar{f}_2 = \frac{1}{n_2} \{X_C f_C + X_N f_N + X_O f_N\}$$

$$f_C = 0$$

$$f_N = \frac{1}{\Sigma_N} \left(18\ e^{-10.452/kT}\right)\ 4.69^{-2}$$

$$f_O = \frac{1}{\Sigma_O}\left\{\left(18\ e^{-9.283/kT}\right)\ 2.16^{-2} + \left(24\ e^{-10.830/kT}\right)\ 2.78^{-3}\right\}$$

$$\bar{\gamma}_2 = \frac{1}{n_2 \bar{f}_2}\ \left\{X_C^{1/2}(\gamma_C f_C)^{1/2} + X_N^{1/2}(\gamma_N f_N)^{1/2} + X_O^{1/2}(\gamma_O f_O)^{1/2}\right\}^2$$

$$(\gamma_C f_C)^{1/2} = 0$$

$$(\gamma_N f_N)^{1/2} = \left(\frac{1}{\Sigma_N}\right)^{1/2}\ \left\{\left(18\ e^{-10.452/kT}\right)^{1/2}\ 7.78^{-11}\right\}$$

$$(\gamma_O f_O)^{1/2} = \left(\frac{1}{\Sigma_O}\right)^{1/2}\ \left\{\left(8\ e^{-9.283/kT}\right)^{1/2}\ 2.62^{-11} + \left(24\ e^{-10.830/kT}\right)^{1/2}\ 1.24^{-11}\right\}$$

$$\bar{\alpha}_2 = \frac{n_2 \bar{f}_2^{\,2}}{\left\{X_C\left(f_C^2/\gamma_C\right) + X_N\left(f_N^2/\gamma_N\right) + X_O\left(f_O^2/\gamma_O\right)\right\}}$$

$$\left(f_C^2/\gamma_C\right) = 0$$

$$\left(f_N^2/\gamma_N\right) = \left(\frac{1}{\Sigma_N}\right)\left(18\ e^{-10.452/kT}\right)\ 3.54^{16}$$

$$(f_0^2/\gamma_0) = (\frac{1}{\Sigma_0}) \{(8\ e^{-9.283/kT})\ 1.59^{16} + (24\ e^{-10.830/kT})\ 1.41^{14}\}$$

$$n_2 = 6X_N + 5X_O$$

$$D_2 = 1.355$$

$$(h\nu)_2 = 3.40$$

GROUP 3

$$\bar{f}_3 = \frac{1}{n_3} \{X_C f_C + X_N f_N + X_O f_O\}$$

$$f_C = \frac{1}{\Sigma_C} \{(9.0)\ 3.88^{-1} + (5\ e^{-1.264/kT})\ 7.29^{-2} + (e^{-2.684/kT})\ 1.98^{-1}\}$$

$$f_N = \frac{1}{\Sigma_N} (6\ e^{-3.576/kT})\ 6.34^{-2} \quad ; \quad f_O = 0$$

$$\bar{\gamma}_3 = \frac{1}{n_3^2 \bar{f}_3} \{X_C^{1/2}(\gamma_C f_C)^{1/2} + X_N^{1/2}(\gamma_N f_N)^{1/2} + X_O^{1/2}(\gamma_O f_O)^{1/2}\}^2$$

$$(\gamma_C f_C)^{1/2} = (\frac{1}{\Sigma_C})^{1/2} \{(9.0)^{1/2}\ 1.67^{-11} + (5\ e^{-1.264/kT})^{1/2}\ 9.08^{-12} + (e^{-2.684/kT})^{1/2}\ 1.05^{-10}\}$$

$$(\gamma_N f_N)^{1/2} = (\frac{1}{\Sigma_N})^{1/2} \{(6\ e^{-3.576/kT})^{1/2}\ 7.63^{-12}\} \quad ; \quad (\gamma_O f_O)^{1/2} = 0$$

$$\bar{\alpha}_3 = \frac{n_3 \bar{f}_3^2}{\{X_C(f_C^2/\gamma_C) + X_N(f_N^2\ \gamma_N) + X_O(f_O^2/\gamma_O)\}}$$

$$(f_C^2/\gamma_C) = (\frac{1}{\Sigma_C}) \{(9.0)\ 3.98^{20} + (5\ e^{-1.264/kT})\ 4.70^{18} + (e^{-2.684/kT})\ 6.22^{18}\}$$

$$(f_N^2/\gamma_N) = (\frac{1}{\Sigma_N})\ (6\ e^{-3.576/kT})\ 4.41^{18} \quad ; \quad (f_O^2/\gamma_O) = 0$$

$$n_3 = 8X_C + X_N$$

$$D_3 = 2.000$$

$$h\nu_3 = 7.000$$

GROUP 4

$$\bar{f}_4 = \frac{1}{n_4} \{X_C f_C + X_N f_N + X_O f_O\}$$

$$f_C = \frac{1}{\Sigma_C} \{(9.0)\ 1.26^{-1} + (5\ e^{-1.264/kT})\ 1.76^{-1} + (e^{-2.684/kT})\ 3.10^{-2}\}$$

$$f_N = \frac{1}{\Sigma_N} \{(10\ e^{-2.384/kT})\ 7.40^{-2} + (6\ e^{-3.576/kT})\ 1.71^{-1}\}$$

$$f_O = \frac{1}{\Sigma_O} (9.0)\ 4.71^{-2}$$

$$\bar{\gamma}_4 = \frac{1}{n_4^2 f_4} \{X_C^{1/2}(\gamma_C f_C)^{1/2} + X_N^{1/2}(\gamma_N f_N)^{1/2} + X_O^{1/2}(\gamma_O f_O)^{1/2}\}^2$$

$$(\gamma_C f_C)^{1/2} = (\frac{1}{\Sigma_C})^{1/2} \{(9.0)^{1/2}\ 3.60^{-11} + (5\ e^{-1.264/kT})^{1/2}\ 7.36^{-10} + (e^{-2.684/kT})^{1/2}\ 5.84^{-10}\}$$

$$(\gamma_N f_N)^{1/2} = (\frac{1}{\Sigma_N})^{1/2} \{(10\ e^{-2.384/kT})^{1/2}\ 8.21^{-12} + (6\ e^{-3.576/kT})^{1/2}\ 3.85^{-11}\}$$

$$(\gamma_O f_O)^{1/2} = (\frac{1}{\Sigma_O})^{1/2} \{(9.0)^{1/2}\ 5.09^{-12}\}$$

$$\bar{\alpha}_4 = \frac{n_4 f_4^2}{\{X_C(f_C^2/\gamma_C) + X_N(f_N^2/\gamma_N) + X_O(f_O^2/\gamma_O)\}}$$

$$(f_C^2/\gamma_C) = (\frac{1}{\Sigma_C}) \{(9.0)\ 2.81^{18} + (5\ e^{-1.264/kT})\ 1.68^{18} + (e^{-2.684/kT})\ 1.66^{14}\}$$

$$(f_N^2/\gamma_N) = (\frac{1}{\Sigma_N}) \{(10\ e^{-2.384/kT})\ 6.00^{18} + (6\ e^{-3.576/kT})\ 7.76^{18}\}$$

$$(f_O^2/\gamma_O) = (\frac{1}{\Sigma_O}) \{(9.0)^{1/2}\ 4.05^{18}\}$$

$$n_4 = 21\ X_C + 6\ X_N + X_O$$

$$D_4 = 2.000$$

$$h\nu_4 = 8.000$$

GROUP 5

$$\bar{f}_5 = \frac{1}{n_5} \{ X_C f_C + X_N f_N + X_O f_O \}$$

$$f_C = \frac{1}{\Sigma_C}\ (9.0)\ 8.65^{-2}$$

$$f_N = \frac{1}{\Sigma_N}\ \{(4.0)\ 1.84^{-1} + (10\ e^{-2.384/kT})\ 1.53^{-1} + (6\ e^{-3.576/kT})\ 6.65^{-2}\}$$

$$f_O = \frac{1}{\Sigma_O}\ \{(5\ e^{-1.967/kT})\ 1.20^{-1} + (e^{-4.188/kT})\ 1.51^{-1}\}$$

$$\bar{\gamma}_5 = \frac{1}{n_5^2 \bar{f}_5}\ \{(X_C)^{1/2}\ (\gamma_C f_C)^{1/2} + (X_N)^{1/2}\ (\gamma_N f_N)^{1/2} + (X_O)^{1/2}\ (\gamma_O f_O)^{1/2}\}^2$$

$$(\gamma_C f_C)^{1/2} = \left(\frac{1}{\Sigma_C}\right)^{1/2} (9.0)^{1/2}\ 2.35^{-10}$$

$$(\gamma_N f_N)^{1/2} = \left(\frac{1}{\Sigma_N}\right)^{1/2} \{(4.0)^{1/2}\ 1.07^{-11} + (10\ e^{-2.384/kT})^{1/2}\ 2.88^{-11} + (6\ e^{-3.576/kT})^{1/2}\ 9.60^{-11}\}$$

$$(\gamma_O f_O)^{1/2} = \left(\frac{1}{\Sigma_O}\right)^{1/2} \{(5\ e^{-1.967/kT})^{1/2}\ 8.86^{-12} + (e^{-4.188/kT})^{1/2}\ 9.93^{-12}\}$$

$$\bar{\alpha}_5 = \frac{n_5 \bar{f}_5^2}{\{X_C(f_C^2/\gamma_C) + X_N\ (f_N^2/\gamma_N) + X_O\ (f_O^2/\gamma_O)\}}$$

$$(f_C^2/\gamma_C) = \frac{1}{\Sigma_C}\ (9.0)\ 2.61^{16}$$

$$(f_N^2/\gamma_N)^2 = \frac{1}{\Sigma_N}\ \{(4.0)\ 5.44^{19} + (10\ e^{-2.384/kT})\ 1.27^{19} + (6\ e^{-3.576/kT})\ 4.77^{16}\}$$

$$(f_O^2/\gamma_O) = \frac{1}{\Sigma_O}\ \{(5\ e^{-1.967/kT})\ 2.21^{19} + (e^{-4.188/kT})\ 3.49^{19}\}$$

$$n_5 = 4X_C + 7X_N + 2X_O$$

$$D_5 = 1.000$$

$$(h\nu)_5 = 10.400$$

GROUP 6

$$\bar{f}_6 = \frac{1}{n_6} \{X_C f_C + X_N f_N + X_O f_O\}$$

$$f_C = \frac{1}{\Sigma_C} (5\ e^{-1.264/kT})\ 7.05^{-1}$$

$$f_N = \frac{1}{\Sigma_N} \{(10\ e^{-2.384/kT})\ 7.89^{-2} + (6\ e^{-3.576/kT})\ 4.55^{-2}\}$$

$$f_O = \left(\frac{1}{\Sigma_O}\right) \{(9.0)\ 1.99^{-2} + (e^{-4.188/kT})\ 1.85^{-2}\}$$

$$\bar{\gamma}_6 = \frac{1}{n_6^2 \bar{f}_6} \{(X_C)^{1/2}\ (\gamma_C f_C)^{1/2} + (X_N)^{1/2}\ (\gamma_N f_N)^{1/2} + (X_O)^{1/2}\ (\gamma_O f_O)^{1/2}\}^2$$

$$(\gamma_C f_C)^{1/2} = \left(\frac{1}{\Sigma_C}\right)^{1/2} (5\ e^{-1.264/kT})^{1/2}\ 6.67^{-11}$$

$$(\gamma_N f_N)^{1/2} = \left(\frac{1}{\Sigma_N}\right)^{1/2} \{(10\ e^{-2.384/kT})^{1/2}\ 1.07^{-10} + (6\ e^{-3.576/kT})^{1/2}\ 2.44^{-11}\}$$

$$(\gamma_O f_O)^{1/2} = \left(\frac{1}{\Sigma_O}\right)^{1/2} \{(9.0)^{1/2}\ 8.56^{-12} + (e^{-4.188/kT})^{1/2}\ 5.46^{-13}\}$$

$$\bar{\alpha}_6 = \frac{n_6 \bar{f}_6^2}{\{X_C (f_C^2/\gamma_C) + X_N\ (f_N^2/\gamma_N) + X_O\ (f_O^2/\gamma_O)\}}$$

$$(f_C^2/\gamma_C) = \frac{1}{\Sigma_C} (5\ e^{-1.264/kT})\ 7.89^{19}$$

$$\left(f_N^2/\gamma_C\right) = \frac{1}{\Sigma_N}\left\{\left(10\ e^{-2.384/kT}\right)\ 6.15^{16} + \left(6\ e^{-3.576/kT}\right)\ 1.90^{17}\right\}$$

$$\left(f_O^2/\gamma_O\right) = \frac{1}{\Sigma_O}\left\{(9.0)\ 1.08^{17} + \left(e^{-4.188/kT}\right)\ 2.12^{19}\right\}$$

$$n_6 = X_C + 7X_N + 2X_O$$

$$D_6 = 1.200$$

$$(h\nu)_6 = 11.500$$